Titre: Title:	Analytical Inference for Visual Inspection Uncertainty in the Context of Transportation Infrastructures
Auteur: Author:	Blanche Laurent
Date:	2022
Type:	Mémoire ou thèse / Dissertation or Thesis
Référence: Citation:	Laurent, B. (2022). Analytical Inference for Visual Inspection Uncertainty in the Context of Transportation Infrastructures [Mémoire de maîtrise, Polytechnique Montréal]. PolyPublie. https://publications.polymtl.ca/10403/

URL de PolyPublie: PolyPublie URL:	https://publications.polymtl.ca/10403/
Directeurs de recherche: Advisors:	James Alexandre Goulet
Programme: Program:	Génie civil

POLYTECHNIQUE MONTRÉAL
affiliée à l'Université de Montréal

Analytical Inference for Visual Inspection Uncertainty in the Context of Transportation Infrastructures

BLANCHE LAURENT
Département de génie civil, géologique et des mines

Mémoire présenté en vue de l'obtention du diplôme de *Maîtrise ès sciences appliquées*
Génie civil

Juillet 2022

POLYTECHNIQUE MONTRÉAL
affiliée à l'Université de Montréal

Ce mémoire intitulé :

Analytical Inference for Visual Inspection Uncertainty in the Context of Transportation Infrastructures

présenté par **Blanche LAURENT**
en vue de l'obtention du diplôme de *Maîtrise ès sciences appliquées*
a été dûment accepté par le jury d'examen constitué de :

Pierre LÉGER, président
Charles L.BÉRUBÉ, membre
James-A. GOULET, membre et directeur de recherche

ACKNOWLEDGEMENTS

I would like to express my deepest and sincerest gratitude to Zachary Hamida, for his support and his countless hours of guidance. I would like to extend my gratitude to my academic advisor Prof. James-A. Goulet, for his counselling and commitment all the way throughout my work. I wish to thank Bhargob Deka for his helpful advices.

I am also grateful to the members of my committee, Prof. Pierre Léger and Prof. Charles L. Bérubé, for their relevant comments and constructive criticisms.

I gratefully acknowledge the assistance of the Transportation Ministry of Quebec Province (MTQ), Canada, for funding this research.

RÉSUMÉ

Les infrastructures de transport se dégradent progressivement tout au long de leur vie, et avec leur vieillissement, il est essentiel de contrôler leur état de dégradation. Les inspections visuelles sont couramment utilisées pour collecter des données sur l'état des infrastructures au fil du temps. La qualité des données d'inspection visuelle dépend de l'expérience de la personne qui effectue la tâche. Certains inspecteurs ont tendance à surestimer ou d'autre vont plutôt sous-estimer l'état de dégradation, ce qui entraîne des difficultés lors de l'interprétation des données. Cette subjectivité dans les évaluations a été partiellement prise en compte dans une approche basée sur des modèles d'espace d'état (SSM), qui quantifie la variance de chaque inspecteur. La principale limite de cette approche est de supposer que tous les inspecteurs sont sans biais. De plus, l'estimation de l'ensemble des paramètres du modèle, y compris l'incertitude des inspecteurs, repose sur une méthode de calcul exigeante basée sur l'optimisation par gradient. Afin d'améliorer l'approche SSM, ce mémoire examine deux points : 1) l'inclusion des biais des inspecteurs dans le modèle d'incertitude afin d'améliorer la capacité de prédiction, et 2) le développement d'une méthode analytique pour réduire le coût de calcul associé à la caractérisation de l'incertitude des inspecteurs. À cette fin, la méthode existante basée sur le gradient est modifiée afin d'estimer et d'inclure les biais des inspecteurs. Après l'estimation du biais, la performance du modèle de dégradation est vérifiée à l'aide de données synthétiques, et validée à l'aide de données réelles. Les résultats de la vérification et de la validation ont montré une amélioration globale de la capacité de prédiction du modèle de dégradation SSM. La méthode analytique permet d'estimer les biais et les variances des inspecteurs en utilisant une approche probabiliste qui s'appuie sur des méthodes Bayésiennes. Les analyses effectuées sur les bases de données synthétiques et réelles ont permis de conclure que la méthode analytique est adéquate pour l'estimation de l'incertitude des inspecteurs, bien qu'elle soit moins precise que celle basée sur le gradient. De plus, l'implantation de celle-ci a permis de réduire le temps de calcul nécessaire à l'estimation de l'incertitude des inspecteurs pour les deux études de cas synthétiques et réelles, ce qui représente une réduction de 33 heures a 20 minutes dans le cas réel. Globalement, nous recommandons d'utiliser l'approche analytique pour estimer l'incertitude des inspecteurs. Malgré une meilleure cohérence des predictions du model de dégradations en utilisant les paramètres estimés par la méthode basée sur l'optimisation par gradient, les estimations faites par la méthodes analytique restent satisfaisantes et le gain en temps de calcul compense la précision réduite.

ABSTRACT

Transportation infrastructure are gradually degrading throughout their life, and with aging, keeping track of their degradation state is essential. Visual inspections are commonly used for collecting data about the state of infrastructures over time. The quality of visual inspection data depends on the experience of the individual performing the task. Some inspectors tend to either over- or underestimate the degradation condition, which leads to difficulties when interpreting the data. This subjectivity in evaluations was partially taken into account in an approach based on state-space models (SSM) that would quantify the variance of each inspector. The main limitation of this existing approach is to assume that all inspectors are unbiased. Moreover, the estimation of the entire set of model parameters, including the inspectors' uncertainty, relies on a computationally demanding gradient-based framework. To improve the SSM-based approach, this thesis examines two points: 1) including the inspectors' biases in the uncertainty model to improve the predictive capacity, and 2) developing an analytical framework to reduce the computational cost associated with the characterization of the inspectors' uncertainty. To that end, the existing gradient-based framework is modified to estimate and include the inspectors' biases. Following the estimation of the bias, the performance of the degradation model is verified using synthetic data, and validated using real data. The verification and validation results have shown an overall improvement in the predictive capacity of the SSM-based degradation model. The analytical framework allows the estimation of the inspectors' biases and variances using a probabilistic approach that relies on Bayesian methods. The analyses performed on the synthetic and real databases have led to the conclusion that the analytical framework is adequate for the estimation of the inspectors' uncertainty, even though it is not as accurate as the gradient-based framework. Furthermore, the implementation of the analytical framework has enabled reducing the computational time required for estimating the inspectors' uncertainty for both the synthetic and real case studies, from 33 hours to 20 minutes in the real case study. Overall, we recommend using the analytical approach for estimating the inspectors' uncertainty. Even though the predictive capabilities of the SSM-KR using the parameters estimated by the gradient-based framework have shown a better consistency, the analytical framework estimations remains satisfactory and the gain in the computational cost compensates for the reduction in accuracy.

TABLE OF CONTENTS

LIST OF TABLES

LIST OF FIGURES

LIST OF SYMBOLS AND ACRONYMS

Symbols

$\boldsymbol{A}$	Transition matrix
$\mathtt{B}$	Total number of bridges
$\mathtt{B}_{\mathtt{tr}}$	Total number of bridges in the training set
$\mathtt{B}_{\mathtt{v}}$	Total number of bridges in the validation set
$\mathtt{B}_{\mathtt{t}}$	Total number of bridges in the test set
$\mathcal{B}$	Bridge identification
$\boldsymbol{C}$	Observation matrix
$\mathcal{D}$	Database of inspections
$\mathtt{E}$	Total number of structural elements
$\mathtt{E}_{\mathtt{t}}$	Number of structural elements in the test set
$\mathtt{E}_{\mathtt{tr}}$	Number of structural elements in the training set
$\mathtt{E}_{\mathtt{v}}$	Number of structural elements in the validation set
e	Structural element identification
$f()$	Probability density function
h	Category of interventions
$\mathcal{I}$	Set of inspectors
$\mathtt{I}$	Total number of inspectors
$\boldsymbol{I}$	Identity matrix
I	Inspector identification
i	Index of inspectors
$\boldsymbol{J}$	Kalman smoother gain matrix
j	Index of bridges
$\boldsymbol{K}$	Kalman gain matrix
$\boldsymbol{k}$	Multivariate kernel function
k	Univariate kernel function
$\mathcal{L}$	Network-scale log-likelihood
l	Lower bound of health condition
ℓ	Kernel length
$\mathtt{M}$	Number of reference points in one dimension
m	Structural attributes index or structural element category index
$\mathcal{N}(\cdot,\cdot)$	Normal distribution

$\mathtt{N}_{ij}$	Number of observed transitions from a state x_i^t to x_j^{t+1}
n	Transformation function shape parameter
o	Transformation function
p	Transition probability or index of structural elements
$p_{1:2}$	Deterioration speed model parameters
$\mathcal{Q}$	Set of bridges
$\mathtt{Q}$	Number of covariates
$\boldsymbol{Q}$	Model process error covariance matrix
$\boldsymbol{R}$	Observation error covariance matrix
$\mathcal{S}$	Structural element category
$\mathtt{S}_j$	Number of structural categories in a bridge j
$\mathtt{T}_p$	Total number of observations
$\mathtt{T}$	Total number of time stamps
t	Time stamp
$\mathcal{U}(\cdot, \cdot)$	Uniform distribution
u	Upper bound of health condition
v	Observation error
$\overline{v}_{s^2}$	Random variable describing the expected value of the square of the observation error
$v_{b(i)}$	Random variable describing the bias of inspectors I_i
$v_{s(i)}$	Random variable describing the standard deviation of inspectors I_i
$\boldsymbol{w}$	Transition model process error
w	Univariate transition model process error
$\overline{w^2}$	Random variable describing $\mathbb{E}[W^2]$
$\boldsymbol{x}$	Vector of hidden states in the unconstrained space
$\tilde{\boldsymbol{x}}$	Vector of hidden states in the constrained space
$\dot{\boldsymbol{x}}_z$	Vector of hidden states associated with covariates
x	State of deterioration condition in the unconstrained space
$\tilde{x}$	State of deterioration condition in the constrained space
$\dot{x}$	State of deterioration speed in the unconstrained space
$\tilde{\dot{x}}$	State of deterioration speed in the constrained space
$\ddot{x}$	State of deterioration acceleration in the unconstrained space
$\tilde{\ddot{x}}$	State of deterioration acceleration in the constrained space
y	Condition observation in the unconstrained space
$\tilde{y}$	Condition observation in the constrained space
$\mathbb{Z}^+$	Set of positive integers
$\boldsymbol{Z}$	Transition probability matrix

$\boldsymbol{Z}_c$	Matrix of reference points
z	Structural attribute
$\boldsymbol{z}_c$	Vector of reference points for a single covariate
δ	Random variable describing the growth in the condition after intervention
$\dot{\delta}$	Random variable describing in the condition after speed
$\ddot{\delta}$	Random variable describing in the condition after acceleration
ϵ	Convergence tolerance
μ	Expected value
$\boldsymbol{\mu}$	Vector of expected values
ν	Iteration limit per parameter
ω	Weight associated with the discrete deterioration state
ρ	Stall limit
σ	Standard deviation
$\boldsymbol{\Sigma}$	Covariance matrix
τ	Intervention time
$\boldsymbol{\theta}$	Vector of model parameters
$\boldsymbol{\theta}^A$	Inspectors' parameters estimated with the analytical framework
$\boldsymbol{\theta}^G$	Inspectors' parameters estimated with the MLE and biased inspectors
$\boldsymbol{\theta}^{G-}$	Inspectors' parameters estimated with the MLE and unbiased inspectors
$\boldsymbol{\theta}^s$	Subset of model parameters
$\boldsymbol{\theta}^v$	Vector of inspectors' parameters
$\boldsymbol{\theta}^k$	Vector of kernel regression parameters
ζ	Initial stall
∞	Infinity

Acronyms

ANN	Artificial Neural Networks
AGVI	Approximate Gaussian Variance Inference
BN	Bayesian Network
CPU	Central Processing Unit
DMM	Discrete Markov Models
GMA	Gaussian Multiplication Approximation
GPU	Graphics Processing Unit
KF	Kalman Filter
KR	Kernel Regression

KS	Kalman Smoother
MLE	Maximum Likelihood Estimation
NR	Newton-Raphson
PDF	Probability Density Function
RBF	Radial Basis Function
SHM	Structural Health Monitoring
SSM	State-Space Model
SSM-KR	Hybrid Model of State-Space Model & Kernel Regression

LIST OF APPENDICES

CHAPTER 1 Introduction

1.1 Motivation

In the context of transportation infrastructures management, one of the main requirements for effective decision-making is to have an accurate metric for the health states of structures over time [3]. Structural health monitoring (SHM) encompass several techniques that enable tracking the performance of bridges and collecting data [3–5]. Those techniques fall under three categories, 1) visual inspection, 2) sensor-based systems and 3) a hybrid of visual inspections and sensor-based systems [6].

Visual inspections is commonly used where inspectors go on-site to grade the condition of the structural elements in a bridge [6]. The main advantage of this method is to provide a general evaluation for the structural condition that is not limited to a specific type of damage [7]. However, visual inspections have major drawbacks that are related to the subjectivity of the evaluation method, as well as the scarcity of inspection data. Visual inspections are carried out by different inspectors with varying capacity at performing the evaluation task, where some inspectors could have a tendency to overestimate the actual degradation state, while others to underestimate it. In addition, the inspections for each bridge are performed by different inspectors over time, with an interval from 2 to 5 years [8].

The aforementioned limitations introduce challenges in interpreting and using the data for modelling the degradation of bridges over time. There are different frameworks for modelling the degradation based on visual inspections [1, 9–13]. State-space models (SSM) have been shown to have the capacity to model the degradation based on visual inspections, while taking into account the uncertainty of inspectors [14]. Nonetheless, the estimation of the inspectors' uncertainty in the SSM framework assumes that the inspectors are unbiased. In addition, the SSM-based model relies on a gradient-based approach for estimating the entire set of model parameters including the inspectors' uncertainty, which is computationally demanding, given the large number of inspections across a network. The aim of this work is to improve the overall predictive capacity of the SSM-based degradation model by estimating the inspectors' biases. Moreover, this thesis examines how to reduce the computational cost associated with the parameter estimation, by providing an analytical framework to estimate the inspectors' uncertainty.

1.2 Network-Scale Monitoring and Visual Inspections

In the context of this research, we consider a SHM database encompassing information about visual inspections data from a network of bridges. This section provides an overview for the network-scale information and the visual inspection method, as well as the inherent limitations of this monitoring method.

1.2.1 Hierarchy of Information within a Network of Bridges

Figure 1.1 shows the hierarchy of information for network-scale monitoring using visual inspections. From Figure 1.1, the network is composed of a set of $\mathtt{B}$ bridges $\mathcal{Q} = \{\mathcal{B}_1, \mathcal{B}_2, ..., \mathcal{B}_{\mathtt{B}}\}$, where each bridges $\mathcal{B}_j$ is composed of a set of structural categories $\mathcal{B}_j = \{\mathcal{S}_1^j, \mathcal{S}_2^j, ..., \mathcal{S}_{\mathtt{S}_j}^j\}$, and each category is composed of structural elements $\mathcal{S}_s^j = \{e_1^j, e_2^j, ..., e_{\mathtt{E}_j}^j\}$. An example of structural category $\mathcal{S}_s^j$ is the category containing all the beam elements within the bridge $\mathcal{B}_j$, other examples could be cables or deckings.

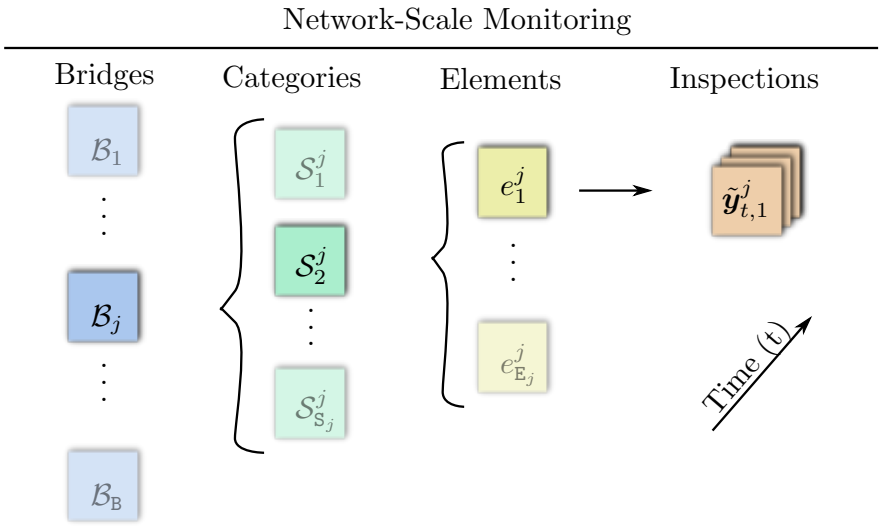

Figure 1.1 Illustration of information hierarchy for network-scale database, where the visual inspections $\tilde{\boldsymbol{y}}$ are performed on the element level of each bridges.

At a given year t, for a given Bridge $\mathcal{B}_j$, the inspections are performed on each bridge's elements by a team of inspectors [8]. During the inspection, the inspector prospects for evidence of defect in the structural elements and assess the severity of their degradation condition [8]. The inspector $I_i \in \{I_1, I_2, ..., I_{\mathtt{I}}\}$ responsable for evaluating element e_p^j, grades the condition $\tilde{y}_{t,p}^j$ on a scale from l to u, where l represents the worst possible condition of the element and u the perfect condition [1].

1.2.2 Visual Inspections Uncertainty

Visual inspections are carried out mainly through the visual observation of the elements, and sometimes backed up by the use of measuring tools or non-destructive tests [8]. The frequency of inspections for a bridge is defined within a range from two to four years depending on structure's age among other factors [8]. Several inspectors can carry out inspections on one element over the years [8]. For example, Figure 1.2 shows an illustration of visual inspections performed on different bridges for a given network.

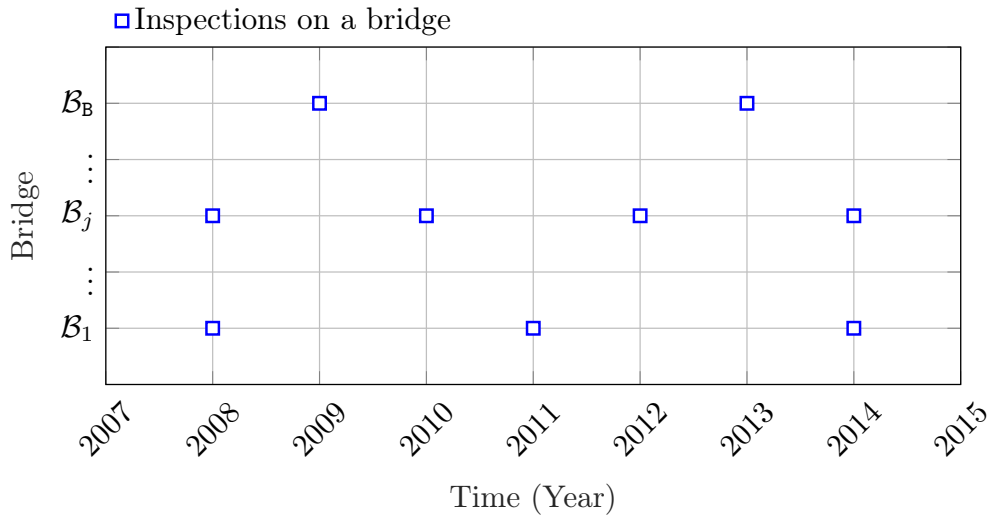

Figure 1.2 Illustration of the distribution of visual inspections performed on different bridges across the network, where each bridge can be inspected by different inspectors $I_{1:\mathtt{I}}$ and at different time intervals.

From Figure 1.2, bridge $\mathcal{B}_j$ has been inspected every two years, while the bridge $\mathcal{B}_{\mathtt{B}}$ is only inspected once every 4 years. As a result, between 2007 and 2015, there are only two inspections available for the elements of bridge $\mathcal{B}_{\mathtt{B}}$. Moreover, as different inspectors are performing inspections on the same element, the uncertainty of each inspector can induce counter-intuitive results. Figure 1.3 shows an Illustration of inconsistencies found within the inspections performed by different inspectors on a single structural element.

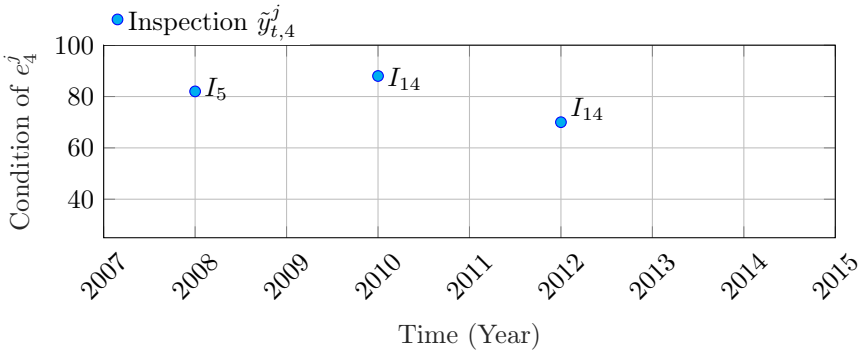

Figure 1.3 Illustration of visual inspections performed on the element e^j_4 of the bridge $\mathcal{B}_j$. Each blue point represents the value of the degradation condition $\tilde{y}^j_{t,4}$ reported by the inspector at a given year.

The data shown in Figure 1.3 presents a typical case that is representative of the variability in the inspection data for an element. From this example, inspector I_5 reported a condition $y^j_{2008,4} = 82$, while the second inspection, performed by Inspector I_{14}, gave a degradation condition, $y^j_{2010,4} = 88$, which is higher than the previous inspection. In the absence of maintenance on the bridge, the element should always degrade from one year to the next. The presence of variability in visual inspection data is common, and can be attributed to the subjective nature of the evaluation, as well as the experience of the inspector in performing the inspection task [15]. Quantifying the uncertainty associated with visual inspection is one of the essential steps for interpreting the inspection data and understanding the degradation of infrastructures over time.

1.3 Research Objectives

The objectives of this research is to improve the performance of the existing SSM-based degradation model. Therefore, this thesis focuses on the following sub-objectives:

- Estimating the inspectors' biases using visual inspection data while relying on the existing gradient-based framework.
- Integrating the inspectors' biases in the degradation model and examining the impact on its overall predictive capacity.
- Reducing the computational time required to perform the estimation of the uncertainty parameters (biases and variances) by developing an analytical inference framework as an alternative for the gradient-based framework.

- Verifying the methods with synthetic data, validating them using real data, and comparing the performance of both frameworks.

1.4 Thesis Outline

The organisation of the thesis is as follows: Chapter 2 presents a literature review, where existing methods and their associated limitations are discussed. Furthermore, Chapters 2 describes the theory of the SSM-based degradation model and the approximate Gaussian variance inference (AGVI) framework, which represents the foundations that this thesis builds upon. Chapter 3 describes the formulation of the proposed frameworks for estimating the inspectors' uncertainty, which includes the estimation of the bias and variance, using two methods; an existing gradient-based method, as well as a new analytical framework. Chapter 4 presents two case studies using synthetic data for verification and real data for validation. The case studies also include a comparison between the gradient-based and the analytical framework. Finally, Chapter 5 concludes the thesis and highlights existing limitations in the proposed framework, as well as future research directions.

CHAPTER 2 Literature Review

2.1 Introduction

This chapter describes the theoretical concepts of existing methods for modelling the degradation condition of structural elements based on visual inspection, as well as their limitations. These models are *Discrete Markov Models* (DMM), regression-based models, and methods that rely on Bayesian updating. Thereafter, the SSM-based degradation model is presented along with potential improvements on the model performance

2.1.1 Modelling Degradation Using Discrete Markov Models (DMM)

DMMs rely on a discrete set of system states and the probabilities of transitioning to a state at time $t+1$ knowing the state at time t [16]. In the context of visual inspections, a time step represents a year, the states represent degradation conditions, and the probabilities are function of the environmental exposure, traffic and unusual extreme events.. For instance, Figure 2.1 shows four degradation states, *Excellent* (x_1), *Good* (x_2), *Damaged* (x_3) and *Seriously Damaged* (x_4).

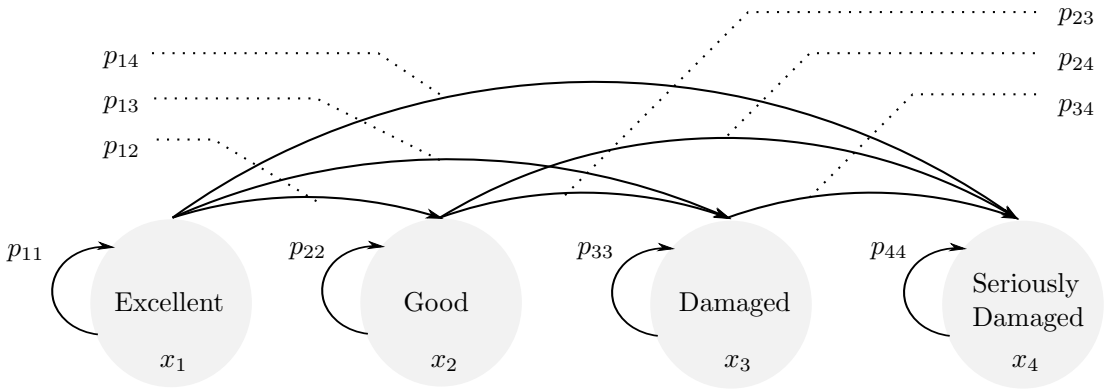

Figure 2.1 Discrete Markov model states with the arrows representing all the possible transitions in a degradation model. Reproduced from [1].

An element can transition from a state x_i at time t, to another state x_j at time $t+1$ with a probability $p_{ij} = \Pr(x_j^{t+1}|x_i^t)$. The possible transitions are represented with arrows in the figure and all the corresponding probabilities are gathered in a transition matrix $\boldsymbol{Z} \in [0,1]^{4\times4}$

that is represented by,

$$\boldsymbol{Z} = \begin{array}{c} \begin{matrix} x_1^{t+1} & x_2^{t+1} & x_3^{t+1} & x_4^{t+1} \end{matrix} \\ \begin{bmatrix} p_{11} & p_{12} & p_{13} & p_{14} \\ 0 & p_{22} & p_{23} & p_{24} \\ 0 & 0 & p_{33} & p_{34} \\ 0 & 0 & 0 & p_{44} \end{bmatrix} \end{array} \begin{matrix} x_1^t \\ x_2^t \\ x_3^t \\ x_4^t \end{matrix} . \tag{2.1}$$

This transition matrix does not include repairs or maintenance so the condition of an element can only degrade over time such that, $p_{ij} = 0,\ \forall i > j$. Moreover, the transition matrix can be simplified by considering that over the course of a year, an element cannot skip a state, so from a state x_i, the element can either stay in this state with a probability of p_{ii} or transition to the next state x_{i+1} with a probability of $1 - p_{ii}$ [10,17]. Accordingly, the transition matrix becomes,

$$\boldsymbol{Z} = \begin{array}{c} \begin{matrix} x_1^{t+1} & x_2^{t+1} & x_3^{t+1} & x_4^{t+1} \end{matrix} \\ \begin{bmatrix} p_{11} & 1-p_{11} & 0 & 0 \\ 0 & p_{22} & 1-p_{22} & 0 \\ 0 & 0 & p_{33} & 1-p_{33} \\ 0 & 0 & 0 & 1 \end{bmatrix} \end{array} \begin{matrix} x_1^t \\ x_2^t \\ x_3^t \\ x_4^t \end{matrix} . \tag{2.2}$$

The probabilities p_{ii} are typically estimated using Maximum Likelihood Estimation (MLE) [18], where the log-likelihood $\mathcal{L}(.)$ is defined by,

$$\mathcal{L}(p) = \sum_{i,j}^{\mathtt{X}} \mathtt{N}_{ij} log(p_{ij}),$$

where $\mathtt{N}_{ij}$ is the number of observed transitions from state x_i^t to state x_j^{t+1}, and $\mathtt{X}$ is the number states. Considering the constraint $\sum_{j=1}^{\mathtt{X}} p_{ij} = 1$, maximizing $\mathcal{L}(.)$ can be done using the *Lagrange multiplier* [18], and by estimating

$$\hat{p_{ij}} = \frac{\mathtt{N}_{ij}}{\sum_{j=1}^{\mathtt{X}} \mathtt{N}_{ij}},$$

where the hat denotes an estimate. Different methods are described to improve the estimation of p_{ij} and the predictive capacity of the model in the context of using visual inspection data [10, 11, 17, 19, 20]. However, DMMs have major drawbacks related to the limited capacity at accounting for the subjectivity of the inspectors. Theoretically, the inspectors' uncertainty could be modelled using an observation matrix for each inspector in a *Hidden Markov Model* [21]. Nevertheless, this method requires considering additional parameters

associated with each of the new observation matrices. In practice, the amount of data necessary for estimating the additional parameters is larger than what is available in common visual inspection databases. Other limitations in the DMMs framework are the presence of approximation errors due to the discretization of the condition and the inability to model the speed of the degradation [22].

2.1.2 Regression Methods

Regression-based methods have also been applied to model the degradation of infrastructures using visual inspection data [12]. A regression approach consists in modelling the relation between covariates $\boldsymbol{z}$ and system responses $\boldsymbol{y}$, through a function $\boldsymbol{y} = g(\boldsymbol{z})$. Artificial neural networks (ANN) is one of the common regression approaches for modelling degradation based on inspection data [9, 23–25]. ANNs relies on a multi-layer framework composed of an input layer, hidden layers and an output layer [26]. Each layer is composed of a set of nodes or hidden nodes linked together by weights. Activation functions can be added to add non-linearities. The weights of ANN are learned by comparing the output from the last layer with the target output to obtain the error, which is propagated back in the layers to update the weights [26]. Choosing the number of layers, nodes and the nature of activation functions is not straightforward, and depends on the context of the application. Moreover, there are additional challenges when applying ANNs in the context of visual inspections, such as, 1) the limited number of observations available per structural element, 2) the unbalanced representation of the degradation condition in the network, and 3) structural attributes selection [1, 23, 27, 28]. As described in Section 1.2, a single element can have few information available concerning its degradation condition over the years, which results in a limited amount of data for the ANN model to be trained efficiently. Moreover, training an ANN on unevenly distributed structural condition may lead to biases in the ANN model estimates. In practice, this is challenging because most bridges are maintained in good condition.
Furthermore, existing ANNs applications have for the most part overlooked the inspectors' uncertainty. This is because ANN requires additional adjustments to include and estimate the uncertainty associated with each inspector. Existing studies that considered the inspectors' uncertainty have relied on external analyses on the inspectors' performance to define a global uncertainty model for the entire set of inspectors [23]. Finally, learning the regression model parameters is usually an offline process, so the model needs to be retrained whenever new data is acquired, making the analysis time consuming.

2.1.3 Bayesian Methods

Another approach for modelling the degradation of infrastructure is by relying on Bayesian methods [1, 13, 29–36]. These methods depend on Bayes rule to update the posterior probability density function (PDF) of a hidden state x, using a prior knowledge and the available observations $\mathcal{D} = \{y_1, ..., y_{\mathtt{D}}\}$ [18], such that,

$$p(x|\mathcal{D}) = \frac{p(\mathcal{D}|x)p(x)}{p(\mathcal{D})}, \tag{2.3}$$

where $p(x|\mathcal{D})$ is the posterior PDF of x knowing $\mathcal{D}$, $p(\mathcal{D}|x)$ is the likelihood function of having the observations $\mathcal{D} = (y_1, ..., y_{\mathtt{D}})$ when the value of x is known, $p(x)$ is the prior density of x and $p(\mathcal{D})$ is the marginal density of $\mathcal{D}$ also known as the evidence.

There are different variations where Bayesian methods are applied to improve the interpretability of the data, as well as the predictive capacity of the degradation models, especially by using different source of data and identifying the factors influencing the quality of visual inspection data [32, 36]. One of the common approachs are Bayesian Networks (BN), which have been applied in the context of health monitoring [32, 37, 38]. The purpose of the BN framework is to model the probabilistic dependencies among different variables or covariates [39]. An example of application is aircraft maintenance, where BNs have been employed to improve the interpretability of visual inspections [32]. In the context of SHM, BNs have been implemented to enable factoring information about structural covariates (e.g., traffic load) to improve the predictive capacity of a DMM degradation model [13, 30, 33, 38].

In the context of visual inspections, state-space models (SSM) has been applied effectively to model the the degradation condition of bridges, while enabling the estimation for the degradation speed and acceleration [1]. The SSM framework allows for the estimation of the inspectors' uncertainty as well as incorporating structural attributes in the degradation analysis. Further details about the SSM framework are provided in the next section as this thesis builds upon this framework to improve its predictive capacity.

2.2 Network-Scale Structural Degradation Modelling

This section provides an overview of the network-scale degradation model proposed by [1], along with its strengths and limitations. This method serves as the foundation for the frameworks proposed in this thesis.

2.2.1 Modelling Structural Degradation with SSM-KR

The SSM-KR method is a hybrid framework based on state-space models (SSM) [1], and Kernel regression (KR) [40]. The SSM framework relies on a *transition model* and an *observation model*. The transition model predicts the degradation state at time t, by knowing the degradation state at time $t-1$, such that,

$$\overbrace{\boldsymbol{x}_{t,p}^{j} = \boldsymbol{A}^{ki}\boldsymbol{x}_{t-1,p}^{j} + \boldsymbol{w}_t}^{\text{transition model}},\ \underbrace{\boldsymbol{w}_t : \boldsymbol{W} \sim \mathcal{N}(\boldsymbol{w}; \boldsymbol{0}, \boldsymbol{Q}^{ki})}_{\text{process error}}, \tag{2.4}$$

with $\boldsymbol{x}_{t,p}^{j}$ representing the hidden state vector of the p-th element $\boldsymbol{e}_p^j$ of the j-th bridge $\mathcal{B}^j$, $\boldsymbol{A}^{ki}$ is the transition matrix, $\boldsymbol{w}_t$ is the process-error, and $\boldsymbol{Q}^{ki}$ is the process error covariance matrix. The hidden states that describe the degradation of the element $\boldsymbol{e}_p^j$ are defined by,

$$\boldsymbol{x}_{t,p}^{j} = [x_{t,p}^{j}\ \dot{x}_{t,p}^{j}\ \ddot{x}_{t,p}^{j}]^{\intercal}, \tag{2.5}$$

where $x_{t,p}^{j}$ is the degradation condition of the element $\boldsymbol{e}_p^j$, $\dot{x}_{t,p}^{j}$ is the speed of the degradation, and $\ddot{x}_{t,p}^{j}$ is the acceleration of the degradation. The transition matrix and process-error covariance matrix are described by,

$$\boldsymbol{A}^{ki} = \begin{bmatrix} 1 & \Delta t & \frac{\Delta t^2}{2} \\ 0 & 1 & \Delta t \\ 0 & 0 & 1 \end{bmatrix}, \quad \boldsymbol{Q}^{ki} = \sigma_w^2 \begin{bmatrix} \frac{\Delta t^4}{4} & \frac{\Delta t^3}{2} & \frac{\Delta t^2}{2} \\ \frac{\Delta t^3}{2} & \Delta t^2 & \Delta t \\ \frac{\Delta t^2}{2} & \Delta t & 1 \end{bmatrix},$$

where Δt is the time step and σ_w^2 is the transition error variance. The relation between the inspection data $y_{t,p}^{j}$ and the hidden states $\boldsymbol{x}_{t,p}^{j}$ is defined by the observation model,

$$\overbrace{y_{t,p}^{j} = \boldsymbol{C}^{ki}\boldsymbol{x}_{t,p}^{j} + v_t}^{\text{observation model}},\ \underbrace{v_t : V \sim \mathcal{N}(v; 0, \sigma_V^2(I_i))}_{\text{observation error}}, \tag{2.6}$$

where $\boldsymbol{C}^{ki} = [1,\ 0,\ 0]$ is the observation matrix, v_t the observation error associated with the i-th inspector who has performed the inspection of the element e_p^j at time t. Equations 2.4 and 2.6 are used in the prediction and update step of the Kalman filter (KF) [41] to predict the Gaussian state $f(\boldsymbol{x}_{t,p}^{j} \mid y_{1:t-1,p}^{j}) = \mathcal{N}(\boldsymbol{x}_t; \boldsymbol{\mu}_{t|t-1}, \boldsymbol{\Sigma}_{t|t-1})$ at time t, such that,

$$\begin{aligned} \boldsymbol{\mu}_{t|t-1} &= \boldsymbol{A}\boldsymbol{\mu}_{t-1|t-1}, \\ \boldsymbol{\Sigma}_{t|t-1} &= \boldsymbol{A}\boldsymbol{\Sigma}_{t-1|t-1}\boldsymbol{A}^{\intercal} + \boldsymbol{Q}, \end{aligned} \tag{2.7}$$

where $\boldsymbol{\mu}_{t|t} = \mathbb{E}[\boldsymbol{x}_t|y_1, y_2, ..., y_t]$ and $\boldsymbol{\Sigma}_{t|t} = \text{cov}(\boldsymbol{x}_t|y_1, y_2, ..., y_t)$ are the expected value and covariance matrix of the hidden state $\boldsymbol{x}_{t,p}^j$ at time t, knowing all the observation from time 1 up to time $t-1$. The update of the posterior knowledge $f(\boldsymbol{x}_{t,p}^j \mid y_{t,p}^j) = \mathcal{N}(\boldsymbol{x}_t; \boldsymbol{\mu}_{t|t}, \boldsymbol{\Sigma}_{t|t})$ at time t is done following,

$$
\begin{aligned}
\boldsymbol{\mu}_{t|t} &= \boldsymbol{\mu}_{t|t-1} + K_t r_t, \\
\boldsymbol{\Sigma}_{t|t} &= (I - K_t \boldsymbol{C}) \boldsymbol{\Sigma}_{t|t-1}, \\
r_t &= y_t - \widehat{y}_t, \\
\widehat{y}_t &= \boldsymbol{C} \boldsymbol{\mu}_{t|t-1}, \\
K_t &= \boldsymbol{\Sigma}_{t|t-1} \boldsymbol{C}^\intercal G_t^{-1}, \\
G_t &= \boldsymbol{C} \boldsymbol{\Sigma}_{t|t-1} \boldsymbol{C}^\intercal + R.
\end{aligned}
\tag{2.8}
$$

Equations 2.7 and 2.8 are employed recursively to estimate the hidden states at each timestep. Figure 2.2 illustrates the degradation estimation process using the Kalman Filter for the example from Section 1.2.2.

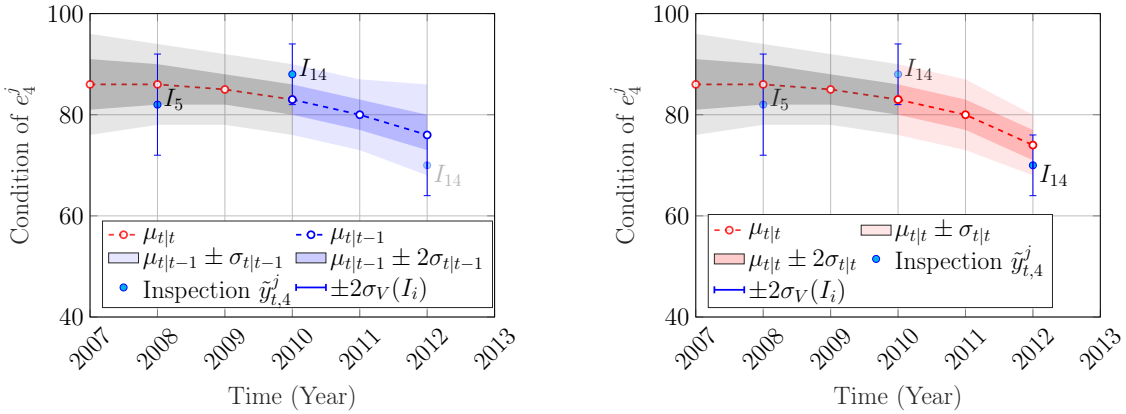

(a) Transition step

(b) Update step

Figure 2.2 Example of degradation estimation of the element e_4^j using the transition and update step of the Kalman Filter from year 2010 to 2012, where the previous degradation states $\mu_{2007:2010}$ are already estimated. Figure 2.2a shows the estimates from the transition model, where the expected value $\mu_{t|t-1}$ is represented in a blue dashed line and the confidence interval for $\sigma_{t|t-1}$ and $2\sigma_{t|t-1}$ are represented by the shaded areas. Similarly, Figure 2.2b shows the model estimates after the update step associated with the inspection performed in 2012, where the expected value $\mu_{t|t}$ is represented in a red dashed line and the confidence interval for $\sigma_{t|t-1}$ and $2\sigma_{t|t-1}$ are represented by the shaded areas. The inspection data is shown by the blue points, where the error bars represents the inspector's uncertainty estimated beforhand.

In this example, the degradation states $\boldsymbol{x}_t$ from year 2007 to 2010 have already been estimated from the inspection data available until 2010. From Figure 2.2a, by using the transition step defined in Equation 2.7 between the years 2010 and 2011, then between 2011 and 2012, the hidden states $\boldsymbol{x}_{2012}$ are forcasted. The new inspection data y_{2012} available in year 2012 is used to update the hidden states using the update step defined in Equation 2.8. Figure 2.2b shows the expected value μ_t represented by a red dashed line and the confidence interval for $\sigma_{t|t}$ and $2\sigma_{t|t}$ represented by the shaded areas. By comparing the estimates from 2.2a and 2.2b, the estimates after the update step is closer to the inspection than before. Moreover, the confidence interval after the transition steps is increasing, this is because the process noise Q is added to the model at each timestep. On the contrary, after the update step, the confidence interval narrows, as adding external information to the model through the inspection and its associated uncertainty enables the model to make more accurate estimations. The standard deviation of each inspector $\sigma_V(I_{1:\mathtt{I}})$, the process-error standard deviation σ_W, the initial degradation condition standard deviation σ_0, and the initial acceleration standard deviation $\ddot{\sigma}_0$ are estimated by relying on the methods described in the Section 2.2.3. Because the number of inspections per element is typically between one and five, it is important to properly define the prior for the hidden states [1]. In the SSM-based degradation model, there are two steps for the initialization of the speed's variance $(\dot{\sigma}^j_{0,p})^2$. The first is to rely on the condition of the structural element such that,

$$(\dot{\sigma}^j_{0,p})^2 = p_1^2(u - \widehat{\mu}_1) + p_2^2,$$

where $\widehat{\mu}_1$ is the expected value of the condition at $t = 1$, and $p_{1:2}$ are model parameters to be estimated. This approximation provides a simple and fast estimation for the initial variance for the speed. However, to improve the predictive capacity of the framework, a second step is applied by using the KR framework, which account for the similarities between bridges. The method relies on taking advantage of the structural similarities (i.e., location, age, material) across the structures to infer the degradation rate. These characteristics are described by different structural attributes $\mathcal{Z} = \{z_1^j, z_2^j, ..., z_{\mathtt{Q}}^j\}$, where each bridge is associated with a vector $\boldsymbol{z}_j$ of $\mathtt{Q}$ covariates. For that end, a grid of $\mathtt{M}$ reference points is employed to discretize the covariates domain, such that, $\boldsymbol{Z}_{\mathtt{c}} = [\boldsymbol{z}_{\mathtt{c}}^1 ... \boldsymbol{z}_{\mathtt{c}}^{\mathtt{Q}}] \in \mathbb{R}^{\mathtt{M}^{\mathtt{Q}} \times \mathtt{Q}}$, where each reference point is associated with an initial speed $\dot{x}_z$ [42]. The initial degradation speed $\dot{x}^j_{0,p}$ of the element e^j_p is then estimated in accordance with the vector $\boldsymbol{z}_j$ associated with the bridge $\mathcal{B}_j$ following,

$$\dot{x}^j_{0,p} = (\boldsymbol{a}^j_p)^{\intercal} \dot{\boldsymbol{x}}_z + w_0, \;\; w_0 : W_0 \sim \mathcal{N}(0, \sigma^2_{w_0}),$$

where $\boldsymbol{a}_p^j$ is a vector of weight defined by,

$$\boldsymbol{a}_p^j = \frac{\boldsymbol{k}(z_j, \boldsymbol{Z}_{\mathtt{c}(m)}, \boldsymbol{\ell})}{\Sigma_{m=1}^{M}(\boldsymbol{k}(z_j, \boldsymbol{Z}_{\mathtt{c}(m)}, \boldsymbol{\ell}))},\ m = 1, ..., \mathtt{M},$$

and $\boldsymbol{k}$ is the multivariate kernel function $\boldsymbol{k} : \mathbb{R}^{\mathtt{Q}} \rightarrow \mathbb{R}$ defined by,

$$\boldsymbol{k}(z_j, \boldsymbol{Z}_{\mathtt{c}(m)}, \boldsymbol{\ell}) = k\left(\frac{z_j^1 - \boldsymbol{z}_{\mathtt{c}(m)}^1}{\ell_1}\right) \cdot ... \cdot k\left(\frac{z_j^{\mathtt{Q}} - \boldsymbol{z}_{\mathtt{c}(m)}^{\mathtt{Q}}}{\ell_{\mathtt{Q}}}\right),\ m = 1, ..., \mathtt{M},$$

where $k(.)$ is the univariate kernel function and $\boldsymbol{\ell} = [\ell_1 ... \ell_{\mathtt{Q}}]$ are the kernel length parameters for each covariate. The vector of hidden states $\dot{\boldsymbol{x}}_z$ is estimated recursively while relying on the Kalman smoother estimates [43]. Moreover, to ensure the monotonicity of the degradation, the speed is constrained in the negative domain using the Gaussian PDF truncation method [44], each time the criterion $\dot{\mu} + 2\dot{\sigma}$ is violated, where $\dot{\mu}$ and $\dot{\sigma}$ are the mean and standard deviation of the speed $\dot{x}$.

Finally, the uncertainty associated with an inspector depends on the current degradation condition of the inspected element. An inspector is unlikely to misjudge the condition when an element is in a perfect or poor condition, while it becomes likely to misjudge a partially damage element because of the subjectivity of the inspections method [45]. To account for the aforementioned phenomena, a non-linear space transformation o is applied on the inspection data [1]. A byproduct of space transformation is to also constrain the degradation condition estimates such that,

$$\begin{aligned} o :& [l, u] \rightarrow \mathbb{R}, \\ & (\tilde{x}, n) \rightarrow x, \end{aligned}$$

where the parameter $n \in \mathbb{Z}^+$ characterizes the shape of the transformation function near the bounds u and l. The notation $\tilde{x}$ represents the state in the constrained space so that $\tilde{x} \in [l, u]$.

Figure 2.3 shows an example where two Normal PDFs are transformed using the space transformation function o, where Figure 2.3a shows the PDFs in the original space $\tilde{x} \in [25, 100]$, Figure 2.3b shows the transformation function o, and Figure 2.3c shows the PDFs after the transformation in the unbounded space $x \in [-\infty, \infty]$. In Figure 2.3a, the PDF represented by a full line is far from the bounds $[l, u]$, as a result, the corresponding PDF in Figure 2.3c is almost unchanged by the transformation. On the other hand, the expected value of the PDF represented by a dashed line is close to the inferior bound $l = 25$ in the original space, as a result, the PDF is affected during the transformation as shown in Figure 2.3c. More

information about the transformation function is available in Appendix A.

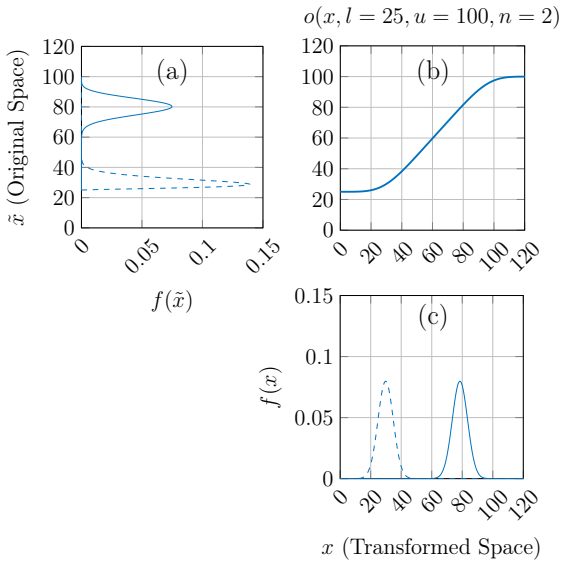

Figure 2.3 Examples of state transformation with the proposed transformation function. Reproduced from [1].

Figure 2.4 outlines how the inspection data is processed from start to finish. The data in the bounded space is transformed to the unbounded space, thereafter, the degradation states are estimated using the SSM-KR framework. Finally, the degradation estimates are transformed to the bounded space to have the final degradation estimates. The parameters to be estimated in the SSM-KR are,

$$\boldsymbol{\theta} = \{\sigma_V(I_{1:I}), \sigma_W, n, \sigma_0, \ddot{\sigma}_0, p_1, p_2, \sigma_{w0}, \boldsymbol{\ell}\}\,.$$

The method used for estimating the set of parameter $\boldsymbol{\theta}$ is described in Section 2.2.3.

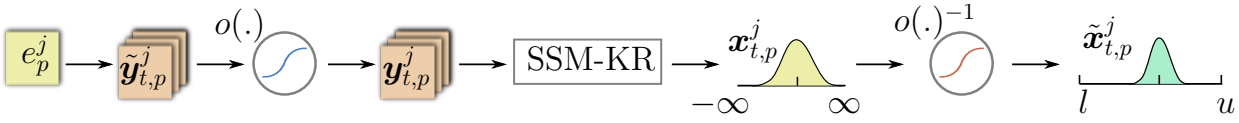

Figure 2.4 Transformation process of the data to estimate the degradation condition of the element $\boldsymbol{e}_p^j$

2.2.2 Effect of Interventions

In addition to estimating the degradation condition over time, it is possible to estimate the effect of interventions on structural elements [1]. An intervention consists in maintenance actions performed on a bridge, such as cleaning or repair activities. These interventions are grouped in categories $h_i, i \in [0, 3]$, and each category induces a specific improvement in the health state of the structural element. The effect of an intervention is described by the variables δ, $\dot{\delta}$ and $\ddot{\delta}$, which are respectively the improvement in the condition, speed and acceleration of the degradation after the intervention. Figure 2.5 shows a synthetic example of the degradation condition and speed over time for element e_1^{53} that underwent intervention.

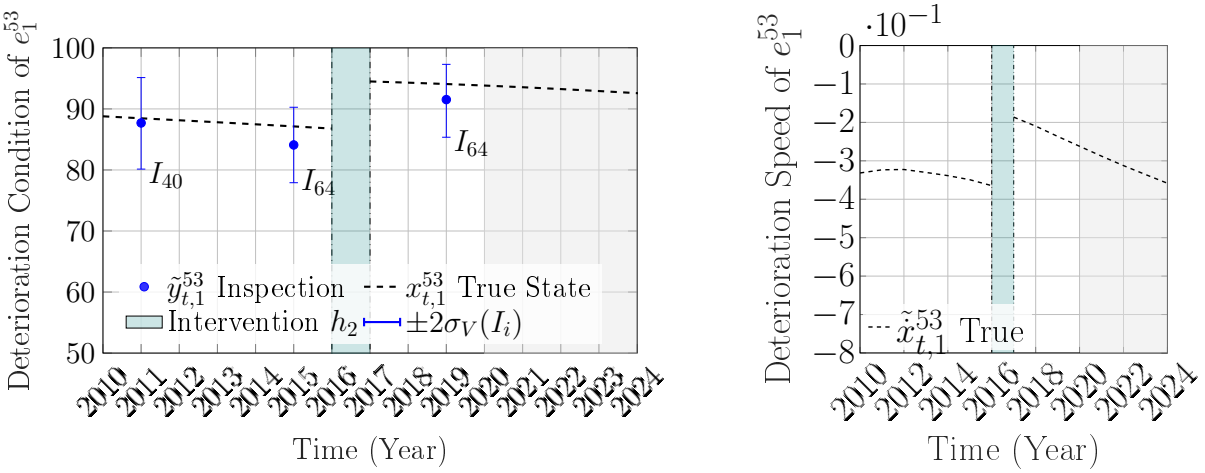

Figure 2.5 Deterioration state example for the condition and the speed of the synthetic structural element e_1^{184}, where an intervention h_2 at time $\tau = 2017$ is represented by the blue area [1].

In this example, the true condition and speed of the element is generated for the purpose of illustration. An intervention from the category h_2 is performed in the year 2017, as a result, the condition of the element after the intervention is higher than before the intervention, by $\delta = 6$ on the condition scale. Similarly, the speed of the degradation is affected by the intervention by $\dot{\delta} = 0.2$ on the speed scale. By using an intervention database, the variables δ, $\dot{\delta}$ and $\ddot{\delta}$ are estimated as hidden states along with the other hidden states of the SSM-KR framework [1].

2.2.3 Parameter Estimation of the SSM-KR Model

The estimation method employed to learn the parameters $\boldsymbol{\theta}$ from the inspection database relies on the *Maximum Likelihood Estimation* (MLE) [46]. The MLE consists in maximizing the joint prior probability of observations given parameters $\boldsymbol{\theta}$, while assuming that all the observations are conditionally independent given the states. The log-likelihood for the entire network of bridges is,

$$\mathcal{L}(\boldsymbol{\theta}) = \sum_{j=1}^{\mathtt{B}} \sum_{p=1}^{\mathtt{E}_j} \sum_{t=1}^{\mathtt{T}_p} \ln f(y_{t,p}^j | y_{1:t-1,p}^j, \boldsymbol{\theta}), \tag{2.9}$$

where $\mathtt{B}$ is the total number of bridges, $\mathtt{E}_j$ is the total number of structural elements for the j-th bridge, $\mathtt{T}_p$ is the total number of observations for the p-th element and $\boldsymbol{\theta}$ is the vector of model parameters. The objective is to optimize all the parameters in $\boldsymbol{\theta}$, such that,

$$\begin{aligned} \boldsymbol{\theta}^* = \underset{\boldsymbol{\theta}}{\operatorname{argmax}}\ & \mathcal{L}(\boldsymbol{\theta}), \\ \text{subject to}: \ & \sigma_V^2(I_i) > 0, \forall I_i \in \mathcal{I}, \\ & n \in [1,2,3,4,5], \\ & \sigma_W, n, \sigma_0, \ddot{\sigma}_0, p_1, p_2, \sigma_{w0}, \boldsymbol{\ell} > 0. \end{aligned}$$

It is possible to solve the above mentioned problem using the Newton-Raphson algorithm within an iterative gradient-based framework [47]. The gradient-based framework relies on two steps for estimating the model parameters. The first step is to optimize the parameters $\boldsymbol{\theta}^s = \{\sigma_W, n, \sigma_0, \ddot{\sigma}_0, p_1, p_2, \sigma_{w0}, \sigma_V\}$, which provides initial values for the variance of each insector σ_V^2, as well as the parameters associated with the initial speed and acceleration. Once the first set of parameter is estimated, the set $\boldsymbol{\theta}^v = \{\mu_V(I_{1:\mathtt{I}}) = 0, \sigma_V(I_{1:\mathtt{I}})\}$ which includes the standard deviations of all the inspectors is estimated with an initial value of σ_V for each inspector, while the parameters $\boldsymbol{\theta}^s$ remain fixed. Finally, the set $\boldsymbol{\theta}^k = \{\sigma_{w0}, \boldsymbol{\ell}\}$ which include the KR model parameters is optimized. These steps are repeated until the improvement in the log-likelihood is less than 0.001.

The main limitation of the gradient-based approach is the computational cost, especially as the number of inspectors increases. The visual inspections database is composed of thousands of bridges, which amounts to days of computations when estimating the model parameters. Moreover, as new inspections are performed every year, the parameters need to be estimated again to take into account the new data. To resolve these limitations, we aim to estimate the inspectors' standard deviation along with the other hidden states using an analytical approach. The next section presents the *Approximate Gaussian Variance Inference* method which enables the inference of the noise variance parameter of the transition model in SSM.

This framework is used in this thesis to replace the NR framework for the estimation of the inspectors variance.

2.3 Approximate Gaussian Variance Inference

This section begins by describing the theoretical basis of the AGVI method for estimating the error process noise. This is followed by a simple case study to illustrate the estimation process using AGVI.

2.3.1 Theoretical Foundation of Univariate AGVI

The *Approximate Gaussian Variance Inference* (AGVI) method is an analytically tractable online Bayesian inference method developed to estimate the error variance parameter σ_W^2 defined in Equation 2.4 [2]. In this section, to simplify the notation, the vector of hidden states $\boldsymbol{x}_{p,t}^j$ describing the degradation of the element e_p^j at a time t is denoted as $\boldsymbol{x}_t^{ki}$. In the AGVI method, the process error w is considered as a hidden state modelled by the random variable $w : W \sim \mathcal{N}(0, \sigma_W^2)$, and learned along with the other hidden state variables in the KF framework. The vector of random variables describing the kinematic model at time t knowing all the observations y from 1 to t, $\boldsymbol{x}_t^{ki} : \boldsymbol{X}^{ki} \sim \mathcal{N}(\boldsymbol{\mu}^{ki}, \boldsymbol{\Sigma}^{ki})$ is augmented to include the new hidden state $\boldsymbol{x} = [x\ \dot{x}\ \ddot{x}\ w]^\intercal$. The inference of the new hidden state is made by the prediction and update steps from the KF, by exploiting the link between the process noise W, the square of process noise W^2 and σ_W^2, while using the Gaussian multiplication approximation (GMA) [48].
More precisely, by relying on the definition of the variance, σ_W^2 can be defined as $\sigma_W^2 = \text{var}[W] = \mathbb{E}[W^2] - \mathbb{E}[W]^2$; considering that the mean $\mathbb{E}[W]$ is assumed to be zero for the process error, the error variance becomes $\sigma_W^2 = \mathbb{E}[W^2]$. Moreover, the GMA is used to approximate W^2 as a Gaussian variable $w_{t|t}^2 : W^2 \sim \mathcal{N}(\mu^{W^2}, (\sigma^{W^2})^2)$. Thereafter, at any t, the variable W^2 can be derived from W by the following equation,

$$\begin{aligned} \mu_{t|t}^{W^2} &= (\mu_{t|t}^{W})^2 + (\sigma_{t|t}^{W})^2, \\ (\sigma_{t|t}^{W^2})^2 &= 2(\sigma_{t|t}^{W})^4 + 4(\sigma_{t|t}^{W})^2(\mu_{t|t}^{W})^2. \end{aligned} \tag{2.10}$$

The expected value of the square of the process error $\mathbb{E}[W^2]$ can then be modeled as a hyper random variable $\overline{w^2}_{t|t} : \overline{W^2} \sim \mathcal{N}(\mu^{\overline{W^2}}, (\sigma^{\overline{W^2}})^2)$, where it has been demonstrated that, $\mu^{\overline{W^2}} = \mathbb{E}[W^2] = \sigma_W^2$ [2]. Consequently, the error of the process noise σ_W is estimated by updating the hyper variable $\overline{w^2}_{t|t}$, and the variable W can be described using the latent

variable, such that $W_{t|t} \sim \mathcal{N}(0, \mu_{t|t}^{\overline{W^2}})$. From this model and by assuming that σ_W^2 is constant from time $t-1$ to t, the KF prediction step gives the predictive PDF of the hidden state vector,

$$\boldsymbol{\mu}_{t|t-1}^{\boldsymbol{X}} = \begin{bmatrix} \boldsymbol{A}^{ki}\boldsymbol{\mu}_{t-1|t-1}^{X^{ki}} \\ 0 \end{bmatrix}_{t|t-1},$$
$$\boldsymbol{\Sigma}_{t|t-1}^{\boldsymbol{X}} = \begin{bmatrix} \boldsymbol{A}^{ki}\boldsymbol{\Sigma}_{t-1|t-1}^{X^{ki}}(\boldsymbol{A}^{ki})^{\intercal} + \boldsymbol{Q}^{ki} & \boldsymbol{\Sigma}^{\boldsymbol{X}^{ki}W} \\ (\boldsymbol{\Sigma}^{\boldsymbol{X}^{ki}W})^{\intercal} & \mu^{\overline{W^2}} \end{bmatrix}_{t|t-1},$$

where the term $\boldsymbol{\Sigma}^{\boldsymbol{X}^{ki}W}$ is the covariance matrix between $\boldsymbol{X}^{ki}$ and W. This knowledge is also used for the transition of W^2 from time $t-1$ to time t using,

$$\begin{aligned} \mu_{t|t-1}^{W^2} &= \mu_{t-1|t-1}^{\overline{W^2}}, \\ (\sigma_{t|t-1}^{W^2})^2 &= 3(\sigma_{t-1|t-1}^{\overline{W^2}})^2 + 2(\mu_{t-1|t-1}^{\overline{W^2}})^2. \end{aligned} \tag{2.11}$$

Thereafter, the inference of σ_W^2 is performed using two updates steps. The first step gives the posterior PDF $f(\boldsymbol{x}_t|y_{1:t})$ following,

$$\begin{aligned} \boldsymbol{\mu}_{t|t}^{\boldsymbol{X}} &= \boldsymbol{\mu}_{t|t-1}^{\boldsymbol{X}} + \frac{\boldsymbol{\Sigma}_{\boldsymbol{X}Y}}{\sigma_Y^2}(y_t - \mu_Y), \\ \boldsymbol{\Sigma}_{t|t}^{\boldsymbol{X}} &= \boldsymbol{\Sigma}_{t|t-1}^{\boldsymbol{X}} \frac{\boldsymbol{\Sigma}_{\boldsymbol{X}Y}\boldsymbol{\Sigma}_{\boldsymbol{X}Y}^{\intercal}}{\sigma_Y^2}, \\ \mu_Y &= \boldsymbol{C}^{ki}\boldsymbol{\mu}_{t|t-1}^{ki}, \\ \sigma_Y^2 &= \boldsymbol{C}^{ki}\boldsymbol{\Sigma}_{t|t-1}^{ki}\boldsymbol{C}^{ki,\intercal} + \sigma_V^2, \\ \boldsymbol{\Sigma}_{\boldsymbol{X}Y} &= \boldsymbol{\Sigma}_{t|t-1}^{\boldsymbol{X}}\boldsymbol{C}_t^{\intercal}, \end{aligned}$$

where $\boldsymbol{C}_t = \begin{bmatrix} \boldsymbol{C}^{ki} & 0 \end{bmatrix}$. The second step updates the knowledge of $\overline{W^2}$ by using the relationship between $Y_{t|t-1}$, $X_{t|t-1}$, $W_{t|t-1}$, ${W^2}_{t|t-1}$, and ${\overline{W^2}}_{t|t-1}$, as shown in the directed acyclic graph displayed in Figure 2.6. The knowledge of W is known from W^2, as represented in the graph by the solid line, using the Equations 2.10 and the knowledge of W^2 is derived from $\overline{W^2}$ using Equations 2.11.

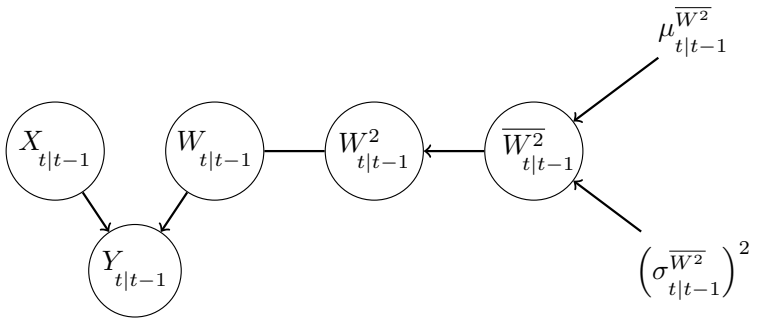

Figure 2.6 Acyclic graph for the online inference of the variance parameter. Reproduced from [2].

Finally the posterior PDF of $\overline{W^2}_{t|t}$ is obtained from $\overline{W^2}_{t|t-1}$, ${W^2}_{t|t}$ and ${W^2}_{t|t-1}$ using,

$$\begin{aligned}\mu^{\overline{W^2}}_{t|t} &= \mu^{\overline{W^2}}_{t|t-1} + K_t(\mu^{W^2}_{t|t} - \mu^{W^2}_{t|t-1}),\\ (\sigma^{\overline{W^2}}_{t|t})^2 &= (\sigma^{\overline{W^2}}_{t|t-1})^2 + (K_t)^2((\sigma^{W^2}_{t|t})^2 - (\sigma^{W^2}_{t|t-1})^2),\end{aligned} \tag{2.12}$$

where, $K_t = \frac{(\sigma^{W^2)}_{t|t-1})^2}{(\sigma^{\overline{W^2}}_{t-1|t-1})^2}$. These steps are repeated for each time step to infer σ^2_W. This method was shown to be computationally efficient, and to provide reliable estimates for the error variance term. The AGVI approach has been only applied to either theoretical toy problems or small-scale time series problems. The next section demonstrates the performance of the AGVI on a simple example problem.

2.3.2 Example for Variance Estimation Using AGVI

The application of the AGVI framework is demonstrated by using a simple example where the true variance is known. In this example, the objective is to estimate the variance of a distribution based on samples from a Normal random variable defined by $W_{\text{true}} \sim \mathcal{N}(0, (\sigma_{W\,\text{true}})^2)$, where $(\sigma_{W\,\text{true}})^2 = 0.5$. To estimate $(\sigma_{W\,\text{true}})^2$, we define the variable $W \sim \mathcal{N}(0, (\sigma_W)^2)$. In this case, the variance of the variable W can be represented by $\mathbb{E}[W^2]$ and is modelled by a random variable $\overline{w^2} : \overline{W^2} \sim \mathcal{N}(\mu^{\overline{W^2}}, (\sigma^{\overline{W^2}})^2)$. The estimation of the variance $(\sigma_W)^2$ is performed by estimating the random variable $\overline{W^2}$.

At the beginning of the estimation process, the initial values for the mean and variance of $\overline{W^2}$ are defined by the prior $\mu^{\overline{W^2}}_0 = 2$ and $(\sigma^{\overline{W^2}}_0)^2 = 1$. Updating the prior of $\mu^{\overline{W^2}}_0$, $(\sigma^{\overline{W^2}}_0)^2$ is done sequentially based on samples from the true distribution W_{true}. The sequential updates starts by updating the expected value $\mu^{W^2}_{t|t}$ and variance $\sigma^{W^2}_{t|t}$ of W^2 using Equations 2.10.

Thereafter, the expected value $\mu^{W^2}_{t|t-1}$ and variance $\sigma^{W^2}_{t|t-1}$ are estimated using the transition defined in Equations 2.11. Using $\mu^{W^2}_{t|t}$, $\mu^{W^2}_{t|t-1}$, $\sigma^{W^2}_{t|t}$, and $\sigma^{W^2}_{t|t-1}$ estimates, it is possible to update the prior PDF of $\overline{W^2}$ by relying on Equations 2.12. The aforementioned operations are repeated recursively for each sample until convergence. It should be noted that in the context of this example the index t is employed as a reference for the sample index.
Figure 2.7 shows the updates on the PDF of $\overline{W^2}$ as represented by the expected value $\mu^{\overline{W^2}}$ and the confidence interval for $\sigma^{\overline{W^2}}$, and $2\sigma^{\overline{W^2}}$, while the true value $(\sigma_{W\,\text{true}})^2 = 0.5$ is represented by a black dashed line.

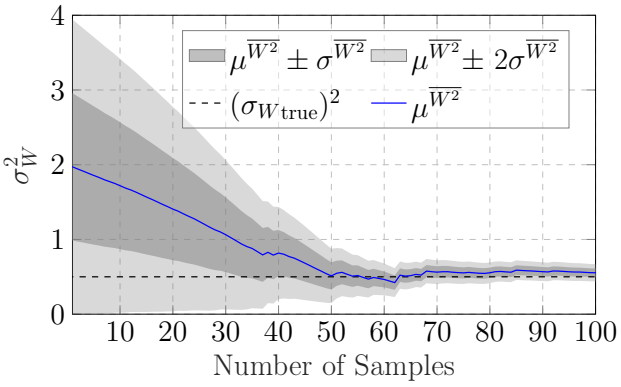

Figure 2.7 Estimation of a standard deviation using the AGVI updates and samples from a Normal distribution $W_{\text{true}} \sim \mathcal{N}(0, (\sigma_{W\,\text{true}})^2)$, where $(\sigma_{W\,\text{true}})^2 = 0.5$ is represented by the dashed line. The mean of the estimated value is represented by the blue line, and the shaded areas represents the confidence intervals for $\sigma^{\overline{W^2}}$, and $2\sigma^{\overline{W^2}}$.

From Figure 2.7, the results show that the AGVI method is able to infer the variance online as samples are being collected. The steps performed in this example can be applied in the context of SSM to estimate the variance associated with the process error.

2.4 Conclusion

This literature review discusses three methodologies to model the degradation condition of structural elements based on visual inspections. The DMM is one of the common approaches for modelling the degradation; however, this framework suffers from disadvantages, such as, the incapacity to take into account the uncertainty associated with each inspector. This is because estimating the inspector's uncertainty is associated with the requirements for estimating additional set of parameters for each inspector; which is infeasible in practice because it requires large amounts of data. In addition, DMM approaches do not allow

quantifying the speed of the degradation.

Another approach for modelling the degradation are regression-based methods which have a limited number of use-cases in the literature in comparison with the DMM models. This is due to having few inspections for each structural element (three or four per element), which introduces challenges in capturing the time dependencies among the observations. Furthermore, as most of the structures are maintained in a good state, it is common to have unbalanced representations for the conditions of the structural elements (i.e., few elements are in a poor condition), which imposes additional challenges on the regression framework. Moreover, the parameter estimation in regression methods is done offline, and requires to train the model again as new data becomes available each year.

The last type of method covered in the literature review is Bayesian methods, specifically, the SSM-based framework. SSM-KR has proven to be efficient in modelling the degradation using visual inspections while taking into account the inspectors uncertainty. However, the SSM-based framework currently relies on an offline procedure for estimating the model parameters, which is computationally demanding. Furthermore, it does not account for the bias of each inspector, which affects the predicting capacity of the model.

In the next chapter, the limitations identified in the SSM-based framework are addressed by using the AGVI framework to estimate the inspectors' standard deviations, in addition to introducing a new framework for estimating the bias. The proposed methods enable reducing the computational cost for estimating the inspectors' uncertainty parameters while having negligible impact on the model predictive capacity.

CHAPTER 3 Methodology

3.1 Introduction

In the existing SSM-based framework, each inspector I_i is associated with a unique observation error, such that $v_{t,p}^j : V(I_i) \sim \mathcal{N}(0, \sigma_V^2(I_i))$, where $\sigma_V^2(I_i)$ is the variance of the i-th inspector. Moreover, the estimation of the inspectors' parameters is performed using a computationally demanding gradient-based framework as described in Section 2.2.
This chapter describes the proposed analytical inference method for estimating the inspectors' uncertainty, which include the biases and the variances, describing the errors made by inspectors. The new observation error is defined by $v_{t,p}^j : V(I_i) \sim \mathcal{N}(\mu_V(I_i), \sigma_V^2(I_i))$, where $\mu_V(I_i)$ is the relative bias associated with inspector I_i.
The chapter starts with a general presentation of the inspectors' relative bias, along with the challenges associated with estimating it. Thereafter, the theoretical foundations of the proposed analytical framework are presented, which include modifications on the state-space model (SSM) and AGVI frameworks. The analytical framework developed in this chapter represents a computationally efficient alternative for the gradient-based framework in estimating the inspectors' uncertainty.

3.1.1 Estimating the Relative Bias of Inspectors

One of the main objectives in this thesis is to enable the estimation of the *relative* bias $\mu_V(I_i)$ of each inspector performing inspections on bridges. The word *relative* implies that while each inspector could have a tendency to overestimate or underestimate the true condition, the average for the biases from all inspectors is zero. Figure 3.1 shows a generic case illustrating how the bias of an inspector affect the observation error distribution. The histogram represents the distribution of the errors for the observations made by the inspector. For an unbiased inspector, the distribution is centered at zero, however, in this case, there is a shift due to the bias. If we try to model the uncertainty associated with this inspector without taking into account the bias, as it is done in the existing framework (Section 2.2), the model will compensate by increasing the standard deviation of the uncertainty (in black doted line in Figure 3.1). Using such a distribution will affect the overall performance of the model. In this thesis, we propose to add the bias of the inspector as a hidden state variable to model the biased error distribution (the blue line Figure 3.1).

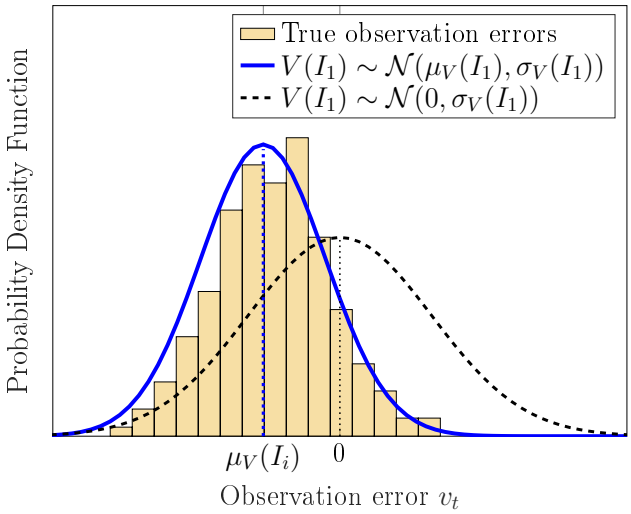

Figure 3.1 Illustration of the observation errors distribution of a biased inspector (yellow histogram) and two corresponding observation models, the first one takes into account the bias $\mu_V(I_i)$ of the inspector (blue line), and the second one considers the bias $\mu_V(I_i) = 0$, (black dashed line).

The estimation of the relative bias for each inspector can be performed using the same MLE method employed for the estimation of SSM-KR model parameters presented in Section 2.2.3. In this context, the set of parameter is increased to include the biases, $\mu_V(I_{1:\mathrm{I}})$. Figure 3.2 presents a flowchart for the estimation of the inspectors' uncertainty using the gradient-based framework. The estimation is performed for one inspector at a time, starting from the initial values $\theta^v = \{\mu_V(I_i) = 0, \sigma_V(I_i) = \sigma_V\}$. The updates in the inspectors' parameters are performed sequentially by maximizing the log-likelihood $\mathcal{L}(\theta^v)$ until convergence, where $\boldsymbol{\theta}^G = \underset{\boldsymbol{\theta}^v}{\operatorname{argmax}} \mathcal{L}(\boldsymbol{\theta}^v)$.

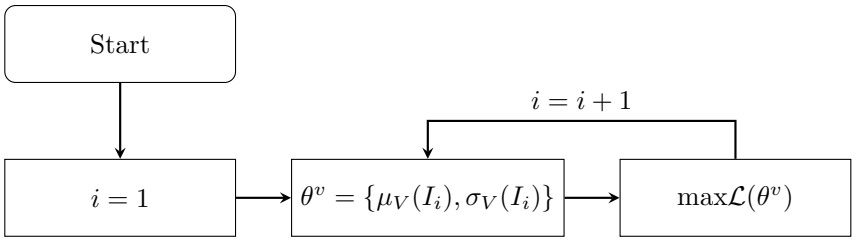

Figure 3.2 Flowchart for the estimation of the inspectors' uncertainty using the gradient-based framework, where the parameters associated with each inspector are estimated in succession.

The pseudo-code which describe the estimation of the inspectors' uncertainty using the gradient-based framework is shown in Appendix B. The main limitation of such an approach is the computational cost. Each parameter needs several epochs over the database to be optimized. Overcoming this limitation is possible by using an analytical inference framework, which is proposed in the next section as an alternative to the gradient-based framework for estimating the inspectors' uncertainty efficiently.

3.2 Analytical Inference of Inspectors' Uncertainty

To infer the bias and the standard deviation, each parameter is represented by a hidden state. In this respect, the observation error term v is represented by two random variables as in,

$$v : V(I_i) = V_b(I_i) + V_s(I_i), \tag{3.1}$$

where $V_b(I_i)$ and $V_s(I_i)$ are employed for modelling the bias and the standard deviation respectively, for any inspector I_i such that,

$$\begin{aligned} v_{b(i)} &: V_b(I_i) \sim \mathcal{N}(v_{b(i)}; \mu_{b(i)}, \sigma^2_{b(i)}), \\ v_{s(i)} &: V_s(I_i) \sim \mathcal{N}(v_{s(i)}; 0, \sigma^2_{s(i)}). \end{aligned} \tag{3.2}$$

It should be noted from Equations 3.1 and 3.2, that taking the bias into consideration introduces additional uncertainty, which can be accommodated by adjusting the estimated variance of the inspector as in, $\sigma^2_V(I_i) = \sigma^2_{b(i)} + \sigma^2_{s(i)}$. The hyper-parameters $\mu_{b(i)}$, $\sigma^2_{b(i)}$ and $\sigma^2_{s(i)}$ fully describe $\mu_V(I_i)$ and $\sigma^2_V(I_i)$, and will be estimated using first a gradient-based framework, then using a new analytical framework.

3.2.1 Inspectors's Uncertainty as Hidden States in Kalman Filter

To infer the hyper-parameters $\mu_{b(i)}$, $\sigma^2_{b(i)}$ and $\sigma^2_{s(i)}$, the variables $v_{b(i),t}$ and $v_{s(i),t}$, are considered as hidden states along with the degradation states of the kinematic model. The hidden state vector is augmented to include the new hidden states,

$$\boldsymbol{x}_t = [\boldsymbol{x}_t^{ki} \;\; v_{b(1)} \;\; v_{s(1)} \;\; ... \;\; v_{b(\mathtt{I})} \;\; v_{s(\mathtt{I})}]^\intercal. \tag{3.3}$$

where $\boldsymbol{x}_t^{ki} = [x_t \;\; \dot{x}_t \;\; \ddot{x}_t]^\intercal$ is the hidden state vector corresponding to the degradation state at time t.

The variables $V_s(I_i)$ and $V_b(I_i)$, are assumed to be independent from each other and from

the degradation state. Furthermore, the biases and standard deviations are assumed to be stationary over time. The observation made on an element is performed by one inspector at a time, so that when an inspection data is available at time t, only the hidden states associated with the inspector I_i are updated. Accordingly, the hidden state vector at time t can be represented by a shorter form,

$$\boldsymbol{x}_t = \begin{cases} [\boldsymbol{x}_t^{ki} \ 0 \ 0]^\intercal & \text{if there is no inspection at time } t, \\ [\boldsymbol{x}_t^{ki} \ v_{b(i)} \ v_{s(i)}]^\intercal & \text{if there is an inspection at time } t, \end{cases}$$

where $i \in [1, \mathtt{I}]$ is the reference number associated with the inspector performing the observation of the element at time t. The mean vector and covariance matrix of the hidden state vector are,

$$\boldsymbol{\mu}_t^{\boldsymbol{X}} = \begin{bmatrix} \boldsymbol{\mu}_t^{ki} \\ \mu_{b(i)} \\ 0 \end{bmatrix}, \qquad \boldsymbol{\Sigma}_t^{\boldsymbol{X}} = \begin{bmatrix} \boldsymbol{\Sigma}_t^{ki} & 0 & 0 \\ 0 & \sigma_{b(i)}^2 & 0 \\ 0 & 0 & \sigma_{s(i)}^2 \end{bmatrix}.$$

At any time t, when there is no observation, the SSM model presented in Section 2.2 is used without changes. However, if there is an observation at time t, the equations of the SSM model are adapted to account for the new hidden states. The transition model for this framework is described by,

$$\boldsymbol{x}_t = \boldsymbol{A}\boldsymbol{x}_{t-1} + \boldsymbol{w}_t, \quad \boldsymbol{w}_t : \boldsymbol{W} \sim \mathcal{N}(\boldsymbol{w}, 0, \boldsymbol{Q}), \tag{3.4}$$

where the transition matrix $\boldsymbol{A}$ is defined by,

$$\boldsymbol{A} = \begin{bmatrix} \boldsymbol{A}^{ki} & \boldsymbol{0}_{2\times2} \\ \boldsymbol{0}_{2\times2} & \boldsymbol{I}_{2\times2} \end{bmatrix}, \quad \boldsymbol{A}^{ki} = \begin{bmatrix} 1 & \Delta t & \dfrac{\Delta t^2}{2} \\ 0 & 1 & \Delta t \\ 0 & 0 & 1 \end{bmatrix},$$

with $\boldsymbol{I}$ representing the identity matrix and $\boldsymbol{A}^{ki}$ is the transition matrix of the kinetic model. The transition error covariance matrix $\boldsymbol{Q}$ is defined by,

$$\boldsymbol{Q} = \begin{bmatrix} \boldsymbol{Q}^{ki} & \boldsymbol{0}_{2\times2} \\ \boldsymbol{0}_{2\times2} & \boldsymbol{0}_{2\times2} \end{bmatrix}, \quad \boldsymbol{Q}^{ki} = \sigma_w^2 \begin{bmatrix} \dfrac{\Delta t^4}{4} & \dfrac{\Delta t^3}{2} & \dfrac{\Delta t^2}{2} \\ \dfrac{\Delta t^3}{2} & \Delta t^2 & \Delta t \\ \dfrac{\Delta t^2}{2} & \Delta t & 1 \end{bmatrix},$$

with $\boldsymbol{Q}^{ki}$ the error covariance matrix of the kinetic model [49]. Using the above-described equation, the prediction step of the KF gives the following PDF for the hidden states, $\boldsymbol{x}_t$: $\boldsymbol{X}_{t|t-1} \sim \mathcal{N}(\boldsymbol{\mu}^{\boldsymbol{X}}_{t|t-1}; \boldsymbol{\Sigma}^{\boldsymbol{X}}_{t|t-1})$, where,

$$\boldsymbol{\mu}^{\boldsymbol{X}}_{t|t-1} = \begin{bmatrix} \boldsymbol{A}^{ki}\boldsymbol{\mu}^{ki}_{t-1|t-1} \\ \mu_{b(i)} \\ 0 \end{bmatrix}, \qquad \boldsymbol{\Sigma}^{\boldsymbol{X}}_{t|t-1} = \begin{bmatrix} \boldsymbol{A}^{ki}\boldsymbol{\Sigma}^{ki}_{t-1|t-1}(\boldsymbol{A}^{ki})^{\intercal} + \boldsymbol{Q}^{ki} & 0 & 0 \\ 0 & \sigma^2_{b(i)} & 0 \\ 0 & 0 & \sigma^2_{s(i)} \end{bmatrix}.$$

The observation model (in Equation 2.6) is also modified accordingly, with $y_t = \boldsymbol{C}\boldsymbol{x}_t$, where $\boldsymbol{C} = [\boldsymbol{C}^{ki}\ 1\ 1]$. The update step of the KF defined in the Equation 2.8 is performed according to the new observation model to update the posterior knowledge $f(\boldsymbol{x}^j_{t,p} \mid y^j_{t,p}) = \mathcal{N}(\boldsymbol{x}_t; \boldsymbol{\mu}_{t|t}, \boldsymbol{\Sigma}_{t|t})$ at time $t-1$ following,

$$\begin{aligned} &\boldsymbol{\mu}_{t|t} = \boldsymbol{\mu}_{t|t-1} + K_t r_t, \\ &\boldsymbol{\Sigma}_{t|t} = (I - K_t\boldsymbol{C})\boldsymbol{\Sigma}_{t|t-1}, \\ &r_t = y_t - \widehat{y}_t, \\ &\widehat{y}_t = \boldsymbol{C}\boldsymbol{\mu}_{t|t-1}, \qquad (3.5) \\ &K_t = \boldsymbol{\Sigma}_{t|t-1}\boldsymbol{C}^{\intercal}G_t^{-1}, \\ &G_t = \boldsymbol{C}\boldsymbol{\Sigma}_{t|t-1}\boldsymbol{C}^{\intercal}. \qquad (3.6) \end{aligned}$$

The variance matrix $\boldsymbol{R}$ is not mentioned explicitly in the equations above, as the observation variance is taken into account implicitely in the hidden state vector. The KF prediction step and update step are used recursively to infer the degradation hidden states, as well as, the inspector biases; however, the estimation of $V_s(I_i)$ is done using the AGVI approach described in Section 3.2.2.

The initialization of the hidden states associated with the inspectors' uncertainty is made using weakly-informative prior for $V_b(I_i)$ and $V_s(I_i)$. The estimation of the aforementioned parameters and the predictive capacity of the framework are updated by using the data over several epochs During each epoch the entire data set available for the training is used to update the inspector's uncertainty. To avoid overfitting on the training set; a cross-validation procedure using an independent validation set is performed throughout the parameter estimation. During the estimation process, the standard deviations $\sigma_{b(i:\mathtt{I})}$ and $\sigma_{s(i:\mathtt{I})}$ are reinitialized using the prior between each epochs to avoid early convergence. During the estimation for the relative bias $\mu_{b(i:\mathtt{I})}$, the expected value for the initial condition $\mu^j_{0,p}$ of each element e^j_p is estimated as a ratio of the maximum observation as, $\mu^j_{0,p} = \left(1 - \frac{\mathbb{E}[\boldsymbol{\mu}_{b(1:\mathtt{I})}]}{u-l}\right) \times \max(\boldsymbol{y}^j_{t,p})$. The aforementioned initialization reduces the possibility of activating the deterioration speed con-

straints (Section 2.2), and is found empirically to yield overall good estimation results. The hidden states associated with the degradation and the inspectors' uncertainty are updated recursively using the KF prediction step, the KF update step, and the AGVI additional update steps, which are presented in Section 3.2.2. In the following section, the AGVI method is modified to infer the standard deviation of the observation error.

3.2.2 Inspector's Variance Estimation Using AGVI

In this section, the AGVI method is employed to infer the inspectors' variance variable $\sigma^2_{s(i:\mathtt{I})}$. Accordingly, the equations used for the inference of σ^2_W presented in Section 2.3 are adapted to the new hidden state $v^2_{s(i)}$. The variable $V^2_s(I_i)$ is approximated as a Gaussian random variable using the GMA and can be derived at any time t from $V_s(I_i)$ using Equation 2.10. The expected value $\mathbb{E}[V^2_s]$ is also considered as a random variable $\overline{v}_{s^2,t} : \overline{V}_{s^2,t|t} \sim \mathcal{N}(\overline{\mu}_{s^2,t|t}, \overline{\sigma}^2_{s^2,t|t})$, allowing the inspector's standard deviation to be parametrizied as,

$$\sigma^2_{s(i)} = \mathbb{E}[V^2_s] = \overline{\mu}_{s^2}.$$

In accordance with the AGVI, the inference of the parameter $\sigma^2_{s(i)}$ is done in two steps. First, the posterior PDF of $f(\overline{v}_{s^2,t}|y_{1:t})$ is obtained through the prediction step and update step of the KF using the matrices presented in Section 3.2.1. This knowledge is used for the transition of V^2_s from time $t-1$ to time t following Equation 2.11. In a second step, the PDF of $\overline{V}_{s^2,t|t}$ is derived from $\overline{V}_{s^2,t|t-1}$, $V^2_{s,t|t}$ and $V^2_{s,t|t-1}$ using Equation 2.12, as shown in the directed acylic graph in Figure 2.6. The hidden states associated with the degradation and the inspectors' uncertainty are updated recursively using the KF prediction step, the KF update step, and the AGVI additional update steps.

3.2.3 The Analytical Framework for Estimating the Inspectors' Uncertainty

Figure 3.3 illustrates the steps for the estimation process using the proposed analytical framework based on the inspection data from a single bridge $\mathcal{B}_j$. The flowchart on the left side shows the sequential updates for the variables $v(I_{1:\mathtt{I}})$ associated with each inspector. For an element $e^j_p \in \mathcal{B}_j$, if an inspection y_t is available at year t, the variable $v(I_i)$ associated with the inspector I_i is updated. The steps for updating $v(I_i)$ for a single inspector I_i at year t, are outlined in the flowchart on the right hand side of Figure 3.3. The first step corresponds to the update of the variables $\overline{v}_{s^2}(I_i)$ and $v_b(I_i)$ using the Kalman update step. Thereafter, the variable $\overline{v}_{s^2}(I_i)$ is updated with the additional AGVI update step. Following the aforementioned update steps, it is possible to obtain v_s from $\overline{v}_{s^2}$, where $\sigma^2_s = \overline{\mu}_{s^2}$ and

$\mu_s = 0$. The resulting estimate for the inspector's uncertainty $v(I_i)$ at time t is computed by the summation of v_b and v_s. These update steps are performed recursively over time for each element in the bridge $\mathcal{B}_j$. To apply the methodology over the entire set of bridges $\mathcal{Q}$, the same process is repeated sequentially for each bridge $\mathcal{B}_j \in \mathcal{Q}$. Further details about the analytical framework are provided in the pseudo-code in Appendix C.

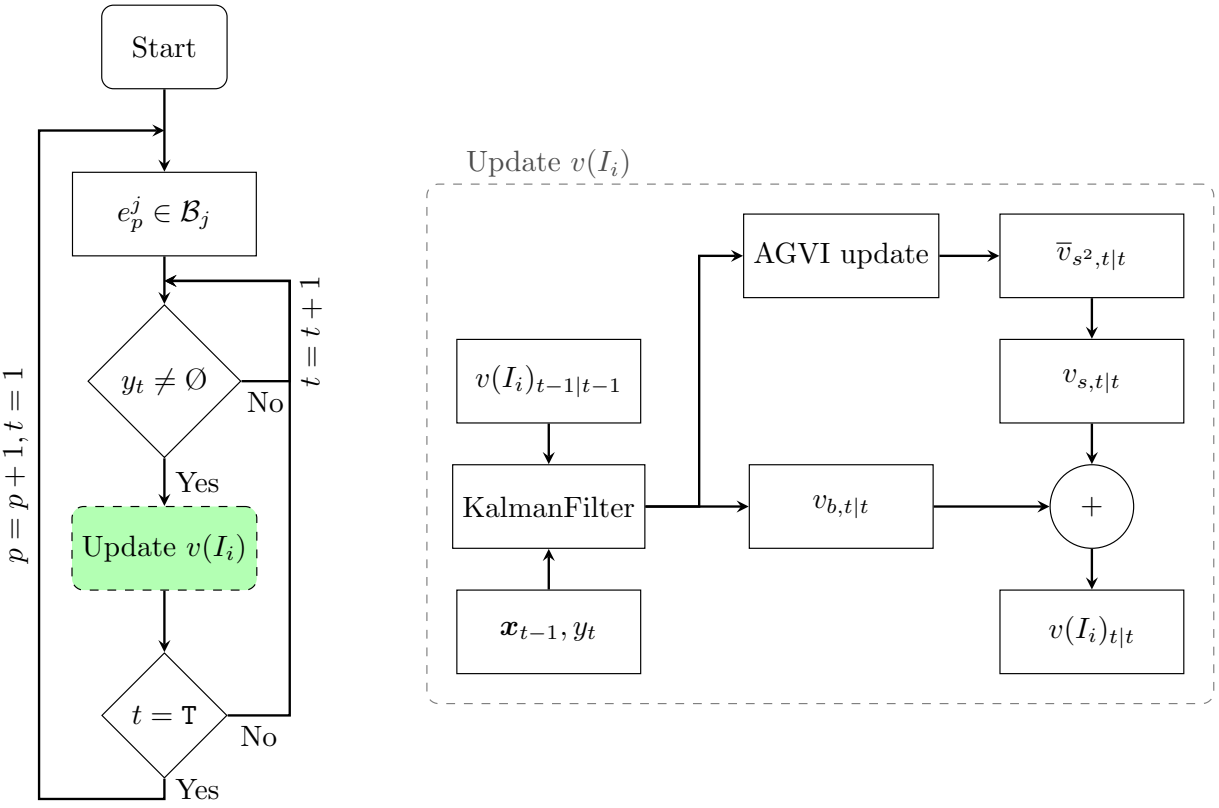

Figure 3.3 Flowchart for the estimation of the inspectors' uncertainty using the analytical framework and the inspection data of a single bridge $\mathcal{B}_j$. On the left, the flowchart presents the iterations performed within the bridge inspection data for estimating the entire set of inspectors' variables $v(I_{i:\mathtt{I}})$. On the right, the flowchart outlines the steps corresponding to the estimation of a single inspector's uncertainty $v(I_i)$ at a given time t.

3.3 Conclusion

In this chapter, a framework is proposed for improving the estimation of the inspectors' uncertainty, and overcoming the limitations identified in Chapter 2. The improvements include modifying the observation model to take into account the bias for each inspector, as

well as the development of an analytical inference framework. In this context, the analytical inference framework represents a computationally efficient alternative to the gradient-based approach for estimating the inspectors' uncertainty. The formulation of the proposed analytical method is based on a recursive procedure for estimating the bias, and the AGVI approach for inferring the inspectors' standard deviations. In the next chapter, the performance of the proposed analytical framework is examined in comparaison to the gradient-based approach. In addition, verification and validation analyses are performed on both of the aforementioned frameworks using synthetic and real data.

CHAPTER 4 Case Study

4.1 Introduction

This chapter presents the results and analyses using two databases; a synthetic one where the true parameters and deterioration states are known, and a real database from the bridge network in the province of Quebec, Canada. These case studies are intended to : 1) quantify the gain of performance obtained by including the inspector's biases into the degradation analyses, and 2) to compare the predictive capacity of the SSM-based model while using the parameters estimated from the analytical framework, as well as the gradient-based framework. In this thesis, the *gradient-based framework* refers to the estimation of the inspectors uncertainty $\boldsymbol{\theta}^v$ using the MLE approach described in Section 2.2.3, while the *analytical framework* refers to the methodology proposed in Chapter 3. In both cases, the remaining model parameters $\boldsymbol{\theta}^s$ and $\boldsymbol{\theta}^k$ that are not associated with inspectors' uncertainty are estimated using the MLE approach.
This chapter is divided into two sections, Section 4.2 presents the verification analyses on the synthetic database, and Section 4.3 presents the validation analyses on the real database. In each of the aforementioned sections, the results concerning the estimation and the inclusion of the inspectors' biases are presented first, followed by a comparaison between the analytical framework and the gradient-based framework.

4.2 Model Verification Using Synthetic Data

The verification of both the analytical and gradient-based framework are performed using synthetic data, where the true condition of the structural elements and true values of the inspectors' parameters are known. This section presents the synthetic database as well as the analysis and results obtained from the gradient-based and the analytical framework.

4.2.1 Synthetic Visual Inspection Data

The synthetic data is tailored to resemble the real data, where the degradation states of $\mathtt{E} = 18000$ synthetic elements are generated, over a lifespan of $\mathtt{T} = 60$ years, using the transition model defined in Equation 2.4. For each structural element, 3 to 5 synthetic inspections are sampled using the observation model defined in Equation 2.6. Other characteristics relating to the degradation condition of the synthetic elements and structural attributes are derived from the work of [14]. For the synthetic database, $\mathtt{I} = 250$ synthetic inspectors are generated,

where each has an observation-error model described by $v_t : V \sim \mathcal{N}(\mu_V(I_i), \sigma_V^2(I_i))$, where $\mu_V(I_i)$ is the bias of inspector I_i, and $\sigma_V^2(I_i)$ is its variance. The biases and variances are generated using a uniform distribution following, $\mu_V(I_i) \sim \mathcal{U}(-4, 4)$ and $\sigma_V(I_i) \sim \mathcal{U}(1, 6)$. Figure 4.1 shows an example of synthetic visual inspections $\boldsymbol{y}_t$ for a single element e_1^{103}, represented by the cyan points, where the black dashed line represents the true degradation condition over 14 years. The true bias $\mu_V(I_i)_{\text{True}}$ associated with each inspector is represented by the shift between the inspection and the observation, so that the correction $y_t - \mu_V(I_i)_{True}$ for the unbiased observations are shown by asterisks. Finally, the error bars represent the inspectors' standard deviations. From Figure 4.1, it is noticeable that in the year 2013 the observation without the bias is closer to the true state. It can happen that an inspector having a negative bias under-estimate the condition due to the variability of his inspection data.

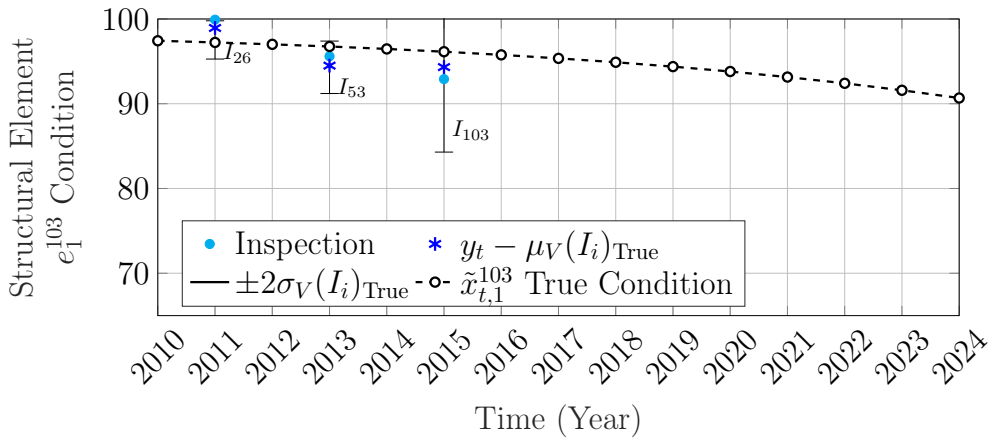

Figure 4.1 An example from the synthetic database of inspections generated using true degradation condition $\tilde{x}_{t,1}^{103}$ of a structural element e_1^{103} performed by biased inspectors.

The verification analysis performed with synthetic data allows assessing the capacity to estimate the inspectors' biases, as well as, comparing the analytical and the gradient-based framework.

4.2.2 Verification Analyses for the Inspectors' Uncertainty Estimated Using the Gradient-Based Framework

Verification analyses are performed to study the capacity of the gradient-based framework to estimate the inspectors' biases, as well as the effects of including the biases on the predictive capacity of the SSM-KR model. In this context, the set of parameters $\boldsymbol{\theta}^G = \{\mu_V(I_i), \sigma_V(I_i)\}$

represents the parameters estimated using the gradient-based framework, while considering the inspectors' biases as model parameters. On the other hand, the set of parameters $\boldsymbol{\theta}^{G-} = \{\sigma_V(I_i)\}$ represents the parameters estimated using the gradient-based framework, while assuming the biases $\mu_V(I_i) = 0$. In both cases, the estimation of the model parameters is done using the MLE approach described in Section 3.1.1. The initial value for the biases is considered $\mu_V = 0$, and the inspectors are assumed to be globally unbiased, so that $\mathbb{E}(\mu_V(I_i)) = 0$. The set of estimated parameters $\boldsymbol{\theta}^G$ is shown in Figure 4.2, where the scatter plots show a comparison between the estimated parameters versus the true values of both the inspectors' standard deviations and biases. The remaining of the SSM-based model parameters are presented in Appendix D.

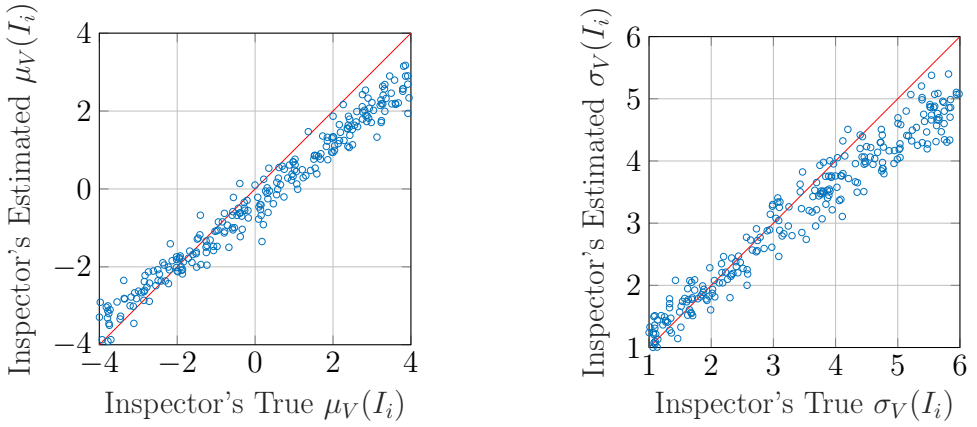

(a) Estimated biases

(b) Estimated standard deviations

Figure 4.2 Results for the estimation of all inspectors' parameters, the biases $\mu_V(I_i)$ (a), and the standard deviations $\sigma_V(I_i)$ (b), compared to their true value using the gradient-based framework.

The coefficient of determination for the estimated biases with the diagonal is $R^2 = 91\,\%$, and the variance of the estimates is $0,5$. In view of these results, it is possible to conclude that the gradient-based framework is effective in estimating the model parameters associated with each inspector. Nonetheless, it is noticeable that there is a deviation in the positive domain for the estimated biases, this can be attributed to the monotonicity of the degradation condition. The predictive capacity of the SSM-KR framework at modelling the elements' degradation, is compared using either the set of parameters $\boldsymbol{\theta}^G$ including the biases, or $\boldsymbol{\theta}^{G-}$ without including the biases. Figure 4.3 shows an example of the degradation analysis of the element e_1^{103}, where the performance of the SSM-KR using both sets are juxtaposed and compared to the true degradation condition. The cyan points correspond to the synthetic inspection data,

and the blue asterisks represent the observations corrected with the bias estimated for each inspector. The black dashed line is the true degradation condition of the elements, while the red dashed line with circle markers is the condition estimated while relying on the set $\boldsymbol{\theta}^{G}$, and the dashed line with squares corresponds to the condition estimates while using $\boldsymbol{\theta}^{G-}$. In this synthetic example, the framework that considers biases is closer to the true state compared with the framework without biases, indicating that the inclusion of the bias in the degradation analyse has improved the predictive performance for this case.

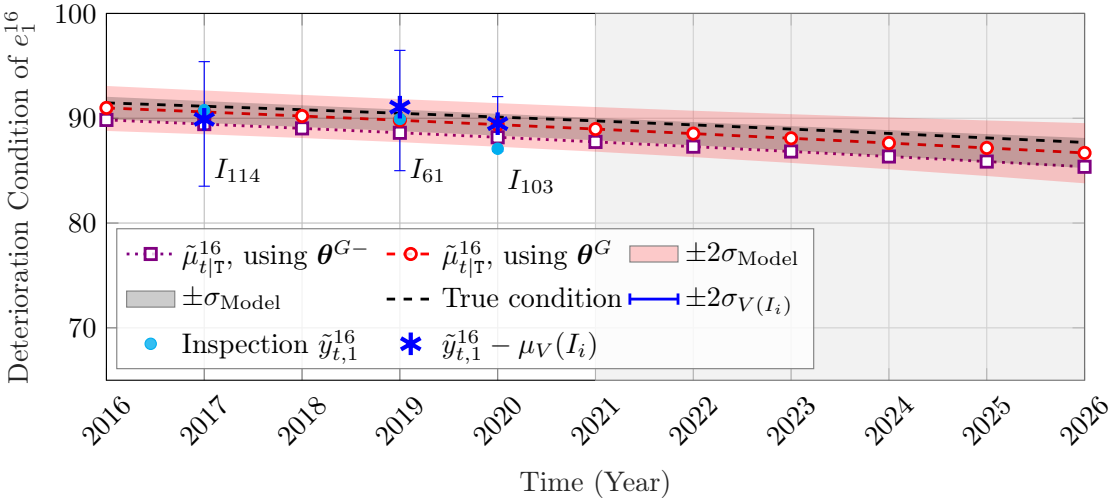

Figure 4.3 Degradation condition analysis from synthetic inspection data $\tilde{y}^{16}_{t,1}$ of a synthetic structural element e_1^{103}. The degradation analysis performed by the SSM-KR using the set $\boldsymbol{\theta}^{G}$ is represented with circle markers, while the one that relies on $\boldsymbol{\theta}^{G-}$ is represented by square violet markers.

To measure the model's overall predictive capacity, we consider the average error for the forecasted conditions and speeds for $\mathtt{E} = 500$ synthetic structural elements, computed following $\sum_{p=1}^{\mathtt{E}}(x^{j}_{t,p} - \mu^{j}_{t|T,p})/\mathtt{E}$, and $\sum_{p=1}^{\mathtt{E}}(\dot{x}^{j}_{t,p} - \dot{\mu}^{j}_{t|T,p})/\mathtt{E}$, respectively. The red lines in Figure 4.4 shows the average forecast error for 10 years while considering the inspectors' biases, and the black dashed lines, without biases, such that $\mu_V(I_i) = 0$, Figure 4.4a presents the results for the condtion and Figure 4.4b for the speed. The light shaded areas represent the confidence interval for the estimation within $\pm 2\sigma$ and the dark one within $\pm\sigma$.

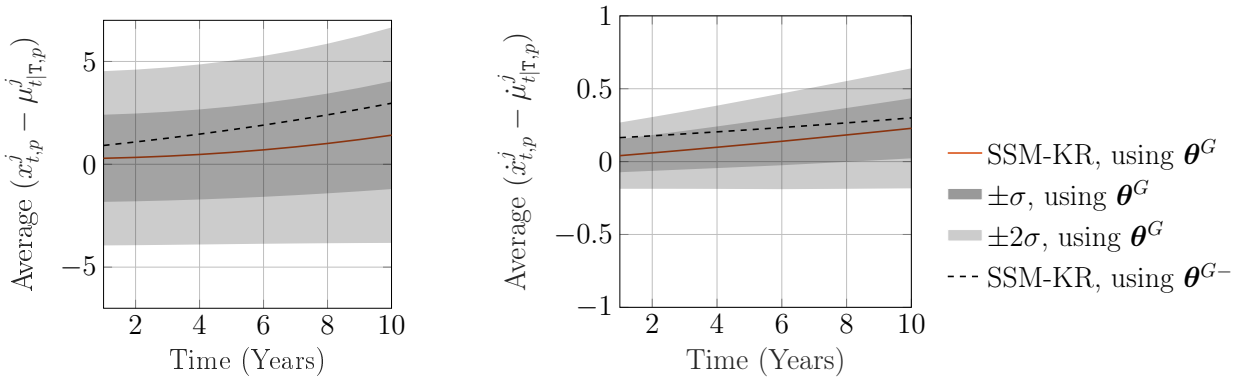

(a) Estimated condition

(b) Estimated speed

Figure 4.4 Average error in forecast for the degradation condition (a) and speed (b), over 10 years, for the gradient-based framework, while including the bias in red, and without biases in black, with the confidence interval for the estimation $\pm 2\sigma$.

The average forecast errors for both the condition and speed are smaller for the framework that accounts for the inspector bias, compared with the one with $\mu_V(I_i) = 0$. Therefore, we can conclude that the inclusion of the biases is improving the overall predictive capacity of the SSM-based framework.

4.2.3 Verification Analyses for the Inspectors' Uncertainty Estimated Using the Analytical Framework

To verify the capacity at estimating the inspectors' uncertainty using the analytical framework, the hidden states variables $\boldsymbol{\theta}^v$ are estimated from the same synthetic data utilized in Section 4.2.2. The set of inspectors' hidden states $\boldsymbol{\theta}^v$ is represented by $\boldsymbol{\theta}^A = \{\mu_b(I_i), \overline{\sigma}_{s^2}(I_i)\}$ when estimated using the analytical framework. The configuration for the analytical framework is identical to the gradient-based framework; however, the analytical framework includes additional hidden states variables, i.e., v_b and $\overline{v}_{s^2}$. The prior for the expected values of the hidden states v_b and $\overline{v}_{s^2}$ are $\mu_b = 0$ and $\overline{\mu}_{s^2} = \sigma_V^2$. The initial values of the variances of the hidden states are assigned large values with $\sigma_b = 1$ and $\overline{\sigma}_{s^2} = 12$. These values are determined empirically through multiple experiments using the synthetic databased to avoid early convergence. An example of application of the analytical inference framework for a single inspector I_{143} is shown in Figure 4.5.

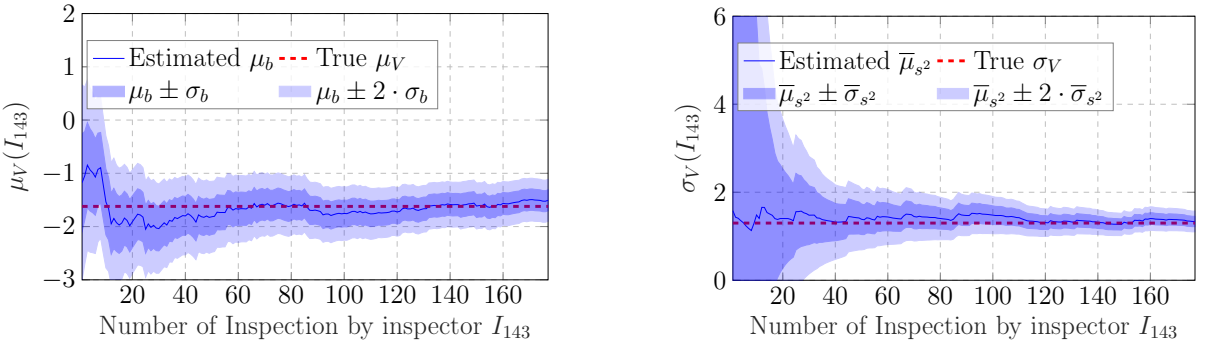

(a) Estimated bias

(b) Estimated standard deviation

Figure 4.5 Estimation process of the uncertainty parameters of inspector I_{143}, the bias $\mu_{b(143)}$ in (a), and the standard deviation $\sigma_{s(143)}$ in (b), using the analytical framework, with the parameters' true value represented by the dashed line, and the blue area representing the uncertainty associated with the estimation.

Figure 4.5a shows the bias estimates from all the observations associated with the inspector I_{143}, where the initial state, defined by $\mu_b = -1,17$ and $\sigma_b = 1,57$, is the result of the last epoch of the analytical inference framework. As explained in Section 3.2, the analytical framework relies on more than one epoch, where the expected values for the hidden state v_b and $\overline{v}_{s^2}$, at the end of one epoch serve as prior for the expected values μ_b and $\overline{\mu}_{s^2}$ for the next epoch, while the standard deviations are reinitialized using their prior $\sigma_b = 1$, and $\overline{\sigma}_{s^2} = 12$. Similarly, Figure 4.5b shows the estimation process of σ_V as updated by the inspection data from inspector I_{143} using the analytical framework. The true values for the bias and standard deviation, which are represented by red dashed lines, are within in the confidence interval of the estimated values which confirms the quality of these estimates.

Figure 4.6 compares the expected values of the estimated hidden states for all inspectors with the true values of the inspectors' uncertainty. The alignment with the diagonal line in Figures 4.6a and 4.6b confirm the capacity of the analytical framework to estimate the inspectors' uncertainty.

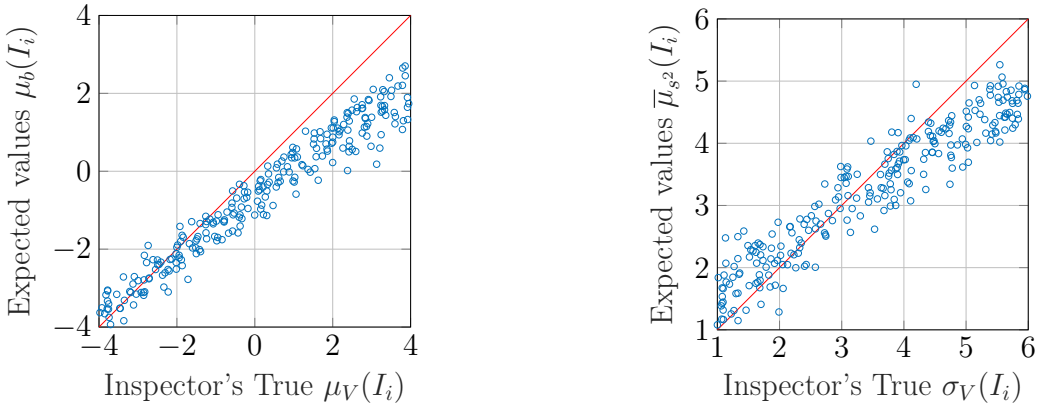

(a) Estimated biases

(b) Estimated standard deviations

Figure 4.6 Results for the estimation of all inspectors' hidden states, the biases $\mu_b(I_i)$ in (a), and the standard deviations $\overline{\mu}_s(I_i)$ in (b), compared to their true value using the analytical framework.

The coefficient of determination for the estimated biases with the diagonal is $R^2 = 76\,\%$, and the variance of the estimates is $0,47$. By comparing the scatter plots from Figure 4.6 and Figure 4.2, it is noticeable that the deviation of the estimates in the positive domain is more importante for the analytical framework than for the gradient-based one. Moreover the deviation for largest standard deviations is explained by the fact that the larger the standard deviation is, the more data is required to estimate it

This is because the analytical bias estimates rely on the degradation condition estimates which are associated with uncertainties, where the gradient-based estimates are obtained through a optimization that is less affected by the knowledge of the degradation condition. It possible to conclude that the estimation of the inspectors' parameters is more accurate for the gradient-based framework, with a reduction of 12 % of the R^2 factor; however, the results from the analytical framework is still consistent with the true parameters' value. Moreover, the hidden states associated with the inspectors' uncertainty are estimated using only 4 epochs compared with a total of 3 000 epochs for the parameters using the gradient-based method (shown in Figure 4.2). This is mainly attributed to the fact that in a single epoch, the analytical inference enables updating the value of all the inspectors' hidden states at once. On the other hand, the gradient-based framework requires multiple epochs for updating the parameters associated with each inspector. Consequently, the computational time associated with estimating the inspectors' parameters is $t_c = 6$ minutes using the analytical framework compared with $t_c = 1140$ minutes using the gradient-based framework, which corresponds to a reduction of 99 % of the computational time.

The estimated values for the other model parameters of the SSM-based framework are reported in Appendix D. The estimation of these parameters is not taken into account in the computational time t_c, as both framework have an identical timing. To evaluate the SSM-KR performance using the aforementioned parameters, Figure 4.7 presents the average forecast errors on the degradation condition and speed over the span of 10 years for both the gradient-based framework (Figure 4.7a) and the analytical framework (Figure 4.7b).

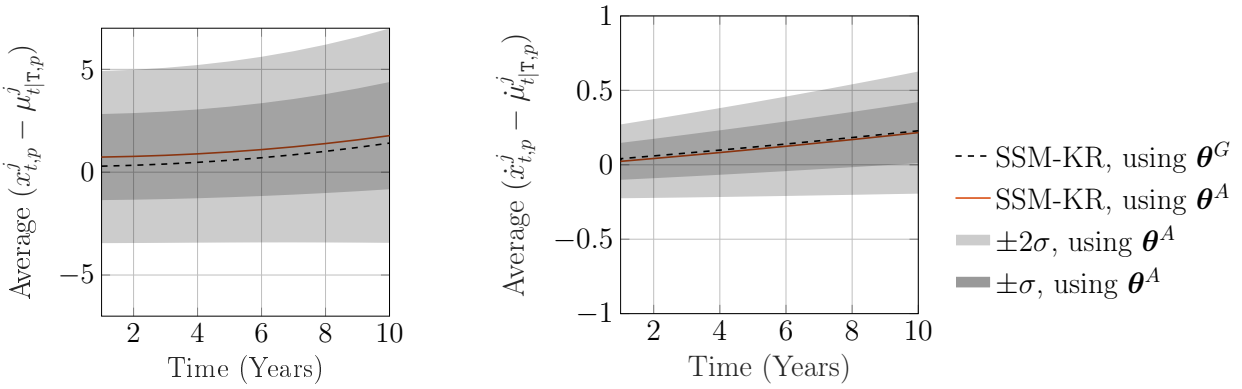

(a) Estimated condition

(b) Estimated speed

Figure 4.7 Average error in forecast for the degradation condition and speed, (a) and (b) respectively, over 10 years, for the analytical framework in red, and gradient-based framework in black, with the confidence interval for the estimation $\pm 2\sigma$.

From Figure 4.7, we can see that the overall average forecast error is approximately the same for the two frameworks, however, the gradient-based framework slightly outperformed the analytical framework by a small margin on the condition's scale. Figure 4.8 shows a scatter plot comparing the true and predicted conditions for 500 synthetic structural elements after 1, 5 and 10 years. The parameters' values $\boldsymbol{\theta}^G$ estimated by the gradient-based framework have led to the condition estimates represented by the blue points, while red points are associated with the SSM-KR that relies on the parameters $\boldsymbol{\theta}^A$ estimated by the analytical framework. Both frameworks have a consistent predictive capacity over time with a slightly higher spread for the estimates obtained from the analytical inference framework.

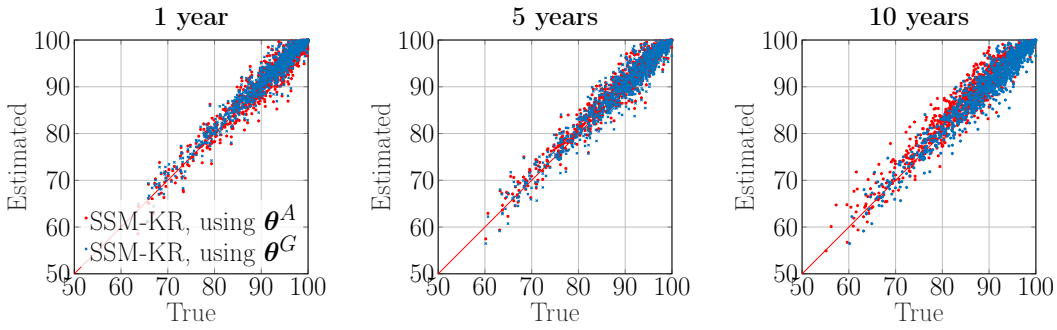

Figure 4.8 Scatter plot of the condition predictions made by the SSM-KR for 500 generated elements after 1, 5 and 10 years. The estimation with the gradient-based framework estimated parameters is presented in blue and for the analytical framework in red.

Based on the verification results in Figure 4.7 and 4.8, it is possible to conclude that the estimation of the inspectors' uncertainty using the analytical framework is comparable to those from the gradient-based framework. In addition the analytical framework significantly reduce the computational cost, and with a negligible effect on the performance of the degradation model (i.e. 99 % of gain in the computational time, and 12 % of loss in accuracy for the bias estimates).

4.3 Model Validation Using Real Data

The validation is performed on a real database from the network of bridges of the province of Quebec, Canada. The database encompasses the inspections performed on the different bridges of the network from 2007 up to 2019. The case study in this thesis specifically considers the visual inspections performed on $\mathtt{E} = 51\,955$ beam structural elements belonging to $\mathtt{B} = 5998$ bridges. The structural attributes $\boldsymbol{z}_j$ employed within the SSM-based framework are: z_j^1 the elements material, z_j^2 the age of the structure, z_j^3 the bridge's location represented by the latitude and z_j^4 the structural element's condition. The selection of the aforementioned attributes is done by estimating the kernel length $\boldsymbol{\ell}$ associated with each structural attribute available in the database, using the MLE approach as described in Section 2.2.3. Thereafter, only the structural attributes with the lowest kernel length relatively to the attribute range of values are considered in the analyses [1]. To perform the parameter estimation, the database is divided into three independent sets of bridges, 1) the training set containing $\mathtt{E_{tr}} = 42\,374$ elements from $\mathtt{B_{tr}} = 1915$ bridges, 2) the validation set with $\mathtt{E_v} = 6\,388$ elements from $\mathtt{B_v} = 142$ bridges, and 3) a test set with $\mathtt{E_t} = 3\,193$ structural elements from $\mathtt{B_t} = 76$ bridges. In this section, the real data is first employed to validate the estimation capacity

of the gradient-based framework for the biases and then, for the validation of the analytical framework.

4.3.1 Quantifying the Inspector's Uncertainty Using the Gradient-Based Framework

The estimation for the model parameters is performed using the MLE approach described in Section 2.2.3. Figure 4.9a and Figure 4.9b show the histograms of the estimated inspectors' parameters $\boldsymbol{\theta}^G$, while Figure 4.9c shows the histogram of the estimated standard deviations based on $\boldsymbol{\theta}^{G-}$ for the framework considering unbiased inspectors. The remaining SSM-based model parameters estimates are presented in Appendix D.
In Figure 4.9a, the average of the estimated biases from all inspectors is 0.12, and is represented by the dashed line. The maximum value of the absolute bias is $\max(|\mu_V(I_i)|) = 3.47$, while the majority of the estimated bias values are between -1 and $+1$. By comparing Figure 4.9b with 4.9c, neglecting the bias enlarges the standard deviation estimates; this is due to the additional variability in the inspection data from inspectors having large bias values.

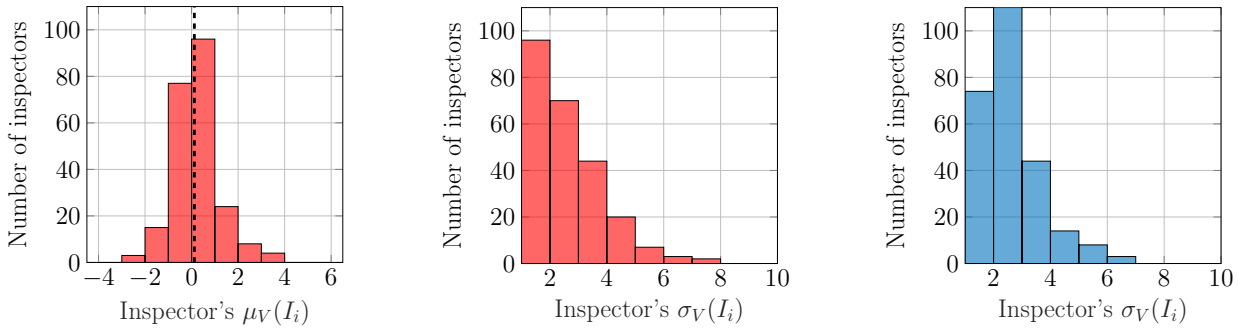

(a) Estimated biases

(b) Estimated standard deviation

(c) Estimated standard deviation while $\mu_V = 0$

Figure 4.9 Histograms for the estimation of the inspectors' parameters in the transformed space for the gradient-based framework. Figure (a) and (b) show the histogram for the estimated biases $\mu_V(I_i)$ and standard deviations $\sigma_V(I_i)$ respectively while considering biased inspectors, while Figure (c) shows the histogram for the estimated standard deviations $\sigma_V(I_i)$, when the inspectors are considered unbiased.

To validate the gradient-based framework, the estimated parameters $\boldsymbol{\theta}^G$ are used to model the degradation of structural elements from the real database. Figure 4.10 shows an example

where the inspection data of element e_{128}^{56} in bridge b_{56} are employed to perform the degradation analysis using the SSM-KR framework and the estimated parameters $\boldsymbol{\theta}^{G}$ and $\boldsymbol{\theta}^{G-}$. Moreover, the last inspection performed on this element in 2019 (represented by a red circle), was removed from the training set to use as a test set and was never used in the estimation of the model parameters nor in the degradation model.

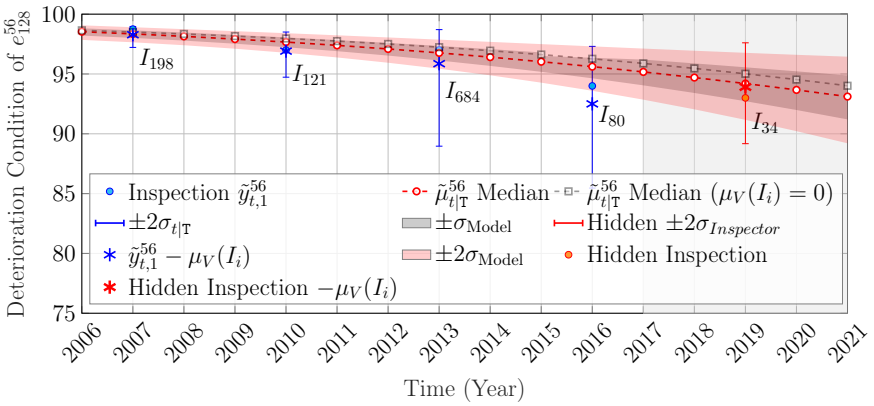

Figure 4.10 Deterioration state analysis for the condition of the structural element e_1^3 based on the inspections $\tilde{\boldsymbol{y}}_{t,1}^{53} \in [25, 100]$. The inspections $\tilde{\boldsymbol{y}}_{t,1}^{53}$ are represented by blue points, where the asterisks represent the correction associated with the estimated bias $\mu_V(I_i)$, and the error bars represent the inspectors' standard deviation. The red point shows the hidden inspection data that was removed from the training data to test the predictive capacity of the SSM-based model. The expected value for the model estimates for the condition $\tilde{\mu}_{t|\mathrm{T}}^{56}$ is shown in red dashed line when $\mu_V(I_i) \neq 0$, and in black when $\mu_V(I_i) = 0$. The red areas represent the confidence interval for σ_{Model} and $2\sigma_{\mathrm{Model}}$ while $\mu_V(I_i) \neq 0$.

In Figure 4.10, to distinguish the bias estimated for each inspector, the observations corrected with inspectors' biases are represented by an asterisk. By comparing the analysis considering biased inspectors (red circle markers) with the one relying on unbiased inspectors (black square markers), the addition of the bias improves the consistency with the hidden observation. Moreover, when the hidden observation is corrected with the inspector's bias, the degradation condition forecast overlaps the hidden observation. The network-scale performance of both analyses considering biased inspectors and unbiased inspectors are reported in Table 4.1, where the log-likelihood associated with the validation and test set are shown. In both cases, the framework showing the best (i.e., the highest) log-likelihood is the one considering biased inspectors.

Table 4.1 Performance comparison for the different frameworks in the log-likelihood associated with the validation and test set.

Model	Log-likelihood	
	Test set	Validation set
Biased inspectors, $\mu_V(I_i) \neq 0$	$-35\,850$	$-67\,916$
Unbiased inspectors, $\mu_V(I_i) = 0$	$-37\,100$	$-68\,410$

4.3.2 Quantifying the Inspector's Uncertainty Using the Analytical Framework

The validation analysis of the analytical framework is performed, first, by comparing the parameters $\boldsymbol{\theta}^A$ estimated using the analytical framework with $\boldsymbol{\theta}^G$ from the gradient-based framework, then, by evaluating the performance of the SSM-based model at predicting the degradation based on the estimated inspectors' uncertainty from $\boldsymbol{\theta}^A$ and $\boldsymbol{\theta}^G$. The inspectors' variables estimated by the analytical framework are reported in Figure 4.11, while the remaining SSM-based model parameters are presented in Appendix D.

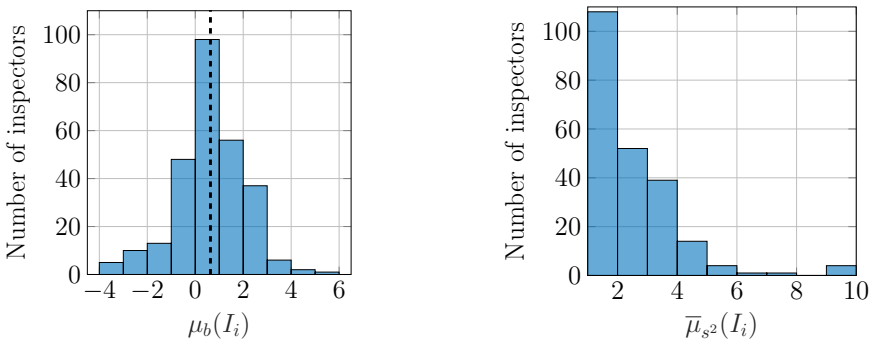

(a) Estimated biases

(b) Estimated standard deviations

Figure 4.11 Histograms for the estimation of the inspectors' variables $\boldsymbol{\theta}^A$ in the transformed space for the analytical framework while considering the relative biases. Figure (a) show the histogram for the estimated biases $\mu_V(I_i)$ and Figure (b), the estimated standard deviations $\sigma_V(I_i)$ respectively.

The average of the estimated biases is equal to 0.63 as represented by the dashed line in Figure 4.11, while the maximum bias value is $\max(|\mu_b(I_i)|) = 5.31$, and most of the estimated bias

values are between -1 and 2. By comparing the results obtained with the gradient-based framework in Figure 4.9, the histogram for the estimated biases is not exactly centered at zero; however, this shift is acceptable considering the range of the estimated bias values. The computational time for both frameworks is reported in Table 4.2. The time associated with the inspectors' variables corresponds to the time required for estimating the inspectors' parameters for all epochs, while the total time is for the estimation of the entire set of model parameters $\boldsymbol{\theta}$, which includes the SSM parameters $\boldsymbol{\theta}^s$, the inspectors' variables $\boldsymbol{\theta}^A$ or $\boldsymbol{\theta}^G$, and the vector of kernel regression parameters $\boldsymbol{\theta}^k$. Replacing the gradient-based framework by the analytical framework in the SSM-based model reduces the total computational time by 42 %. In the gradient-based framework, the estimation of the inspectors' variables represents 44 % of the computational time where for the analytical frameworks it is less than 1 %.

Table 4.2 Comparison for the computational time required for estimating the sets of inspectors' uncertainty $\boldsymbol{\theta}^v$ and model parameters $\boldsymbol{\theta}$ while using the analytical and gradient-based frameworks for estimating $\boldsymbol{\theta}^v$.

Method used for estimating $\boldsymbol{\theta}^v$	Time required for estimating	
	Inspectors' parameters $\boldsymbol{\theta}^v$	All parameters $\boldsymbol{\theta}$
Gradient-based framework	33 hours	75 hours
Analytical framework	0.3 hours	43 hours

To assess the predictive capacity of the SSM-based method using the variables $\boldsymbol{\theta}^A$, the last inspection $\tilde{y}_{\mathtt{T}}$ of the elements where removed from the training set of the degradation model. Figure 4.12a shows a scatter plot comparing the condition states $\tilde{\mu}_{t|\mathtt{T}-1}$ estimated from the data available until $\mathtt{T}-1$ with the corresponding hidden observations $\tilde{y}_{\mathtt{T}}$. Figures 4.12b shows the same scatter plot for the SSM-based model using the parameters $\boldsymbol{\theta}^G$. The forecast period can differ for each structural element, as the number of years between two consecutive inspections is not the same for every bridges. Each type of marker corresponds to the number of years for the forecast period, i.e., the number of years between the last observation used in the training and the hidden observation.

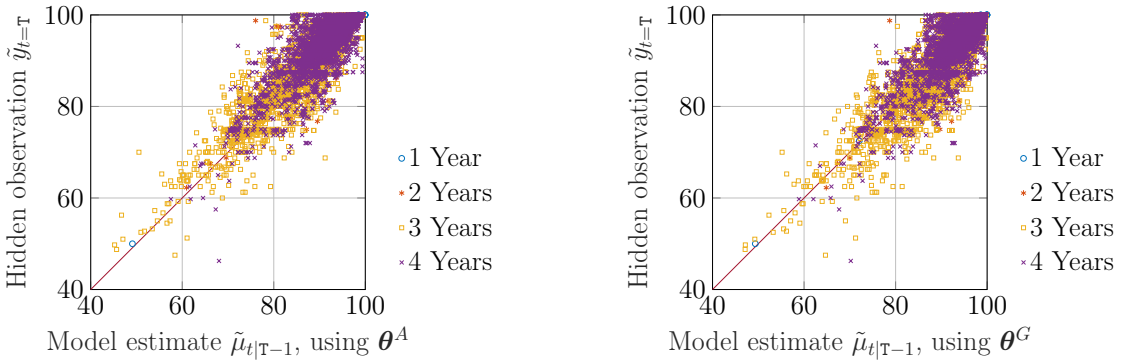

(a) Analytical framework

(b) Gradient-based framework

Figure 4.12 Forecast estimation of the degradation condition versus hidden observation with different forecast period of the SSM-based model using the estimated parameters of the analytical framework $\boldsymbol{\theta}^A$ in Figure (a), and gradient-based frameworks $\boldsymbol{\theta}^G$ in Figure (b).

From Figure 4.12a, the predictive capacity of the SSM-based model shows no difference which respect to the forecast time. The predictions are not required to match the inspection data given that the observations do not represent the true state of the element, which is unobservable in practice. Moreover, by comparing Figure 4.12a with Figure 4.12b, the SSM-based model predictive capacity is not altered by the use of the analytical framework instead of the gradient-based one for estimating the inspectors' uncertainty.
The network-scale performance of the analytical frameworks is evaluated by the log-likelihood for the test set associated with the SSM-KR model while using $\boldsymbol{\theta}^G$ or $\boldsymbol{\theta}^A$, which are reported in Table 4.3. Even though the gradient-based framework shows a better log-likelihood for the test set compared with the analytical framework, the analytical framework's predictive capacity is still acceptable considering the results from Figure 4.12, and the improvements in the computational time shown in Table 4.2.

Table 4.3 Performance comparison for the SSM-based framework in the log-likelihood associated with the test set, while using the estimates from the analytical and gradient-based frameworks.

Parameters used in the SSM-based model	Log-likelihood for the test set
$\boldsymbol{\theta}^G$	$-35\,850$
$\boldsymbol{\theta}^A$	$-36\,220$

4.4 Conclusion

This chapter has presented the verification and validation analyses for the inclusion of the inspectors' bias in the degradation model, and for the estimation of the inspectors' parameters using the analytical framework. Concerning the inclusion of the biases, the analyses carried out on the synthetic data have shown a good performance for the estimation of the inspectors' bias using the gradient-based framework, as well as the analytical framework. Moreover, it has been shown that the consideration of the bias in the degradation model improves the overall predictive capacity of the SSM-KR. The synthetic analyses have also demonstrated the capacity of the analytical framework to estimate the inspectors' parameters, without significantly impacting the SSM-KR performance. In addition, The use of the analytical framework reduces the number of epochs necessary for the estimation compared with the gradient-based framework. The analyses performed using the real database have allowed validating the performance of the model while including the relative bias for each inspector. Even though the estimation of the gradient-based framework is overall more consistent, the analytical framework offers a significant reduction in the computational time while maintaining a marginally inferior performance.

CHAPTER 5 Conclusion

5.1 Thesis Conclusions

This research project has examined the inspectors' uncertainty in the context of visual inspections on transportation infrastructures. To that end, two frameworks were developed for estimating the inspectors' relative biases and standard deviations. The first framework relies on the MLE approach that is already employed for estimating the SSM-based model parameters, while the second framework is based on the AGVI estimation framework as well as the Kalman update step. The verification and validation analyses performed on synthetic and real databases have led to the following conclusions:

1. The inclusion of the inspectors' relative bias in the degradation model improves the predictive capacity of the framework. These improvements are demonstrated by an overall reduction of 61 % on the average forecast errors for the synthetic case, and an increase of 2 % in the log-likelihood for the test set for the real data.

2.a. Both the analytical and gradient-based frameworks proved to be effective in quantifying the inspectors' relative biases.

2.b. The analytical framework implementation provides a significant gain in the computational time required for the inspectors' uncertainty estimation, going from 33 hours to 20 minutes given the computational recourses available for the study, however, the accuracy of the parameters estimation is less than with the gradient-based framework. The total computational time is reduced by 40% for the real data when using the analytical framework for estimating the inspectors' uncertainty.

3. It is possible to infer the variance describing the inspectors' errors analytically using the approximate Gaussian variance inference (AGVI) approach.

Overall, we recommend using the analytical approach for estimating the inspectors' uncertainty. Even though the predictive capacity of the SSM-KR using the parameters estimated by the gradient-based framework have shown a better consistency, the analytical framework estimations remains satisfactory and the gain in the computational cost compensates for the reduced accuracy.

5.2 Limitations

This section highlights some of the limitations of the proposed approach for the estimation of the inspectors' uncertainty.

5.2.1 Initialization for the Relative Biases and Standard Deviations in the Analytical Framework

One of the requirements for estimating the inspectors' uncertainty using the analytical framework is to define the initialization for the hidden states associated with the biases and variances. This is a challenging task due to the limited number of inspections per structural element (i.e., 1 to 6 inspections), as well as the high uncertainty associated with each inspection points. As described in Section 4.2.3, the initial values for each inspector's parameters are defined as, $\mu_b = 0$ and $\sigma_b = 1$ for the bias, and $\overline{\mu}_{s^2} = \sigma_V$ and $\overline{\sigma}_{s^2} = 12$ for the standard deviation. The aforementioned initial values are defined to have a reasonably large variance to prevent restricting the estimation to the initial expected value, and at the same time to avoid early convergence and suboptimal parameters. In general, the initialization for the bias and variance may required performing empirical analyses using synthetic data to determine the values for σ_b and $\overline{\sigma}_{s^2}$ given the range $[l, u]$ of the inspection data, therefore the values provided need to be reconsidered if the range of the inspection data is different (i.e., $[l, u] \neq [25, 100]$).

5.2.2 The Global Bias for all Inspectors

In this thesis, the focus is to estimate the relative bias of each inspectors, where the word *relative* indicates that the bias of one inspector is estimated in comparaison with other inspectors, while assuming that on average they are unbiased. This assumption excludes the possibility that the entire set of inspectors could be globally biased, meaning that on average all inspectors are under- or over-estimating the degradation condition. To estimate the true inspectors' bias, it would be required to include the global bias using an additional hidden state. However, in using such an approach, there are some challenges that remain to be solved related to the non-identifiability of the relative and the global bias [50]. For instance, if the global bias is 2, then all the data available is shift of +2, but with no reference point available to compare the entire database with, it is not possible to estimate the global bias.

5.3 Future Work

This sections suggests possible directions for future work, to improve the degradation framework.

5.3.1 Stationarity of the Observation Model Parameters

In this thesis, all inspectors' parameter $\mu_V(I_i)$ and $\sigma_V(I_i)$ are considered to be stationary. This hypothesis implies that over a long period of time, the inspectors are assumed to maintain the same performance. However, in reality, an inspector can improve his knowledge with more experience, and thus, having more accurate observations from year to year. To account for this phenomenon in the model, the biases and standard deviations of each inspector would need to be considered as non-stationary by formulating a transition model for inspectors' parameters.

5.3.2 Reducing the Computational Cost Associated with Learning the Degradation Model Parameters

The current SSM-KR model includes several parameters that are estimated using the gradient-based framework. Those parameters $\boldsymbol{\theta}^s$ relate to the initial values of the SSM model and $\boldsymbol{\theta}^k$ are associated with the kernel regression framework. The potential for reducing the computational cost is especially high for the $\boldsymbol{\theta}^k$ parameters. The kernel regression has been integrated into the framework to account for the similarity between the structural attributes of each element, and for determining the initial speed of the degradation. To that end, the KR method relies on a state vector $\dot{\boldsymbol{x}}_z$ which is estimated using computationally demanding operations [14]. For example, in the beam database, which contains $\mathtt{E} = 51955$ elements, the computational time for the estimation of the $\boldsymbol{\theta}^k$ parameters is approximately of 17 hours, out of the 43 hours required for estimating all the SSM-KR parameters (i.e., 40% of the total computational time). To improve the usability of the framework, a future work could focus on replacing the KR method with an analytically tractable regression approach, such as the TAGI method [48].

REFERENCES

[1] Z. Hamida and J.-A. Goulet, "Modeling infrastructure degradation from visual inspections using network-scale state-space models," *Structural Control and Health Monitoring*, vol. 27, no. 9, p. e2582, 2020.

[2] B. Deka and J.-A. Goulet, "Online Bayesian inference of process noise in State-Space Models," *In preparation*, 2022.

[3] F. Ansari, *Sensing issues in civil structural health monitoring*. Springer, 2005.

[4] J. M. Brownjohn, "Structural health monitoring of civil infrastructure," *Philosophical Transactions of the Royal Society A: Mathematical, Physical and Engineering Sciences*, vol. 365, no. 1851, pp. 589–622, 2007.

[5] H.-N. Li, L. Ren, Z.-G. Jia, T.-H. Yi, and D.-S. Li, "State-of-the-art in structural health monitoring of large and complex civil infrastructures," *Journal of Civil Structural Health Monitoring*, vol. 6, no. 1, pp. 2190–5479, 2016.

[6] D. Agdas, J. A. Rice, J. R. Martinez, and I. R. Lasa, "Comparison of visual inspection and structural-health monitoring as bridge condition assessment methods," *Journal of Performance of Constructed Facilities*, vol. 30, no. 3, p. 04015049, 2015.

[7] M. M. Lima, D. Miller, and J.-H. Doh, "Structural health monitoring of concrete bridges in Guilan province based on a visual inspection method," *Structural Durability and Health Monitoring*, vol. 9, no. 4, pp. 269 1930–2983, 2013.

[8] *Manuel d'inspection des structures*, Transports Québec, Direction des structures, 2014.

[9] T. J. X.W. Ye and C. Yun, "A review on deep learning-based structural health monitoring of civil infrastructures," *Smart Structures and Systems*, vol. 24, no. 5, pp. 567–586, 2019.

[10] C. Ferreira, L. C. Neves, J. C. Matos, and J. M. S. Soares, "A degradation and maintenance model: Application to portuguese context," *Proceedings of Bridge Maintenance, Safety, Management and Life Extension*, pp. 483–489, 2014.

[11] J. Kalbfleisch and J. F. Lawless, "The analysis of panel data under a Markov assumption," *Journal of the American Statistical Association*, vol. 80, no. 392, pp. 863–871, 1985.

[12] C. R. Farrar and K. Worden, *Structural health monitoring: a machine learning perspective*. John Wiley and Sons, 2012.

[13] M. Li and G. Jia, "Bayesian Updating of Bridge Condition Deterioration Models using Complete and Incomplete Inspection Data," *Journal of Bridge Engineering*, vol. 25, no. 3, pp. 1084–0702, 2020.

[14] Z. Hamida and J.-A. Goulet, "Network-scale deterioration modelling of bridges based on visual inspections and structural attributes," *Structural Safety*, vol. 88, pp. 0167–4730, 2021.

[15] M. Moore, B. M. Phares, B. Graybeal, D. Rolander, G. Washer, and J. Wiss, "Reliability of visual inspection for highway bridges, volume i," Turner-Fairbank Highway Research Center, Tech. Rep., 2001.

[16] L. R. Bellet, *Ergodic properties of Markov processes*. Springer, 2006, pp. 1–39.

[17] G. Fu and D. Devaraj, *Methodology of Homogeneous and Non-homogeneous Markov Chains for Modelling Bridge Element Deterioration*. Michigan Department of Transportation, 2008.

[18] K. Murphy, *Machine Learning: A Probabilistic Perspective*. MIT Press, 2012.

[19] M. Kallen and J. Van Noortwijk, "Statistical inference for Markov deterioration models of bridge conditions in the Netherlands," in *Proceedings of the Third International Conference on Bridge Maintenance, Safety and Management*, no. 16-19, 2006.

[20] C. H. Jackson, "Multi-State models for panel data: the msm package for R," *Journal of Statistical Software*, 2011.

[21] L. Rabiner and B. Juang, "An introduction to hidden Markov models," *IEEE ASSP Magazine*, vol. 3, no. 1, pp. 0740–7467, 1986.

[22] P. L. Durango-Cohen, "A time series analysis framework for transportation infrastructure management," *Transportation Research Part B: Methodological*, vol. 41, no. 5, pp. 0191–2615, 2007.

[23] E. K. Winn, "Artificial neural network models for the prediction of bridge deck condition ratings," Master's thesis, Michigan State University, 2011.

[24] Y.-H. Huang, "Artificial neural network model of bridge deterioration," *Journal of Performance of Constructed Facilities*, vol. 24, no. 6, pp. 0887–3828, 2010.

[25] J. Lee, K. Sanmugarasa, M. Blumenstein, and Y.-C. Loo, "Improving the reliability of a bridge management system (BMS) using an ANN-based backward prediction model (BPM)," *Automation in Construction*, vol. 17, no. 6, pp. 0926–5805, 2008.

[26] M. Ghiassi, H. Saidane, and D. Zimbra, "A dynamic artificial neural network model for forecasting time series events," *International Journal of Forecasting*, vol. 21, no. 2, pp. 341–362, 2005.

[27] R. Matkovskyy and T. Bouraoui, "Application of neural networks to short time series composite indexes: Evidence from the nonlinear autoregressive with exogenous inputs (NARX) model," *Journal of Quantitative Economics*, vol. 17, no. 2, pp. 2364–1045, 2019.

[28] W. Foster, F. Collopy, and L. Ungar, "Neural network forecasting of short, noisy time series," *Computers and Chemical Engineering*, vol. 16, no. 4, pp. 0098–1354, 1992.

[29] M. A. Zanini, F. Faleschini, and C. Pellegrino, "Bridge residual service-life prediction through bayesian visual inspection and data updating," *Structure and Infrastructure Engineering*, vol. 13, no. 7, pp. 906–917, 2017.

[30] E. Arango, M. Santamaria, H. S. Sousa, and M. J. C, *Reliability-Based Bayesian Updating Using Visual Inspections of Existing Bridges*. Springer, 2021.

[31] H. Korving and J. Van Noortwijk, "Bayesian updating of a prediction model for sewer degradation," *Urban Water Journal*, vol. 5, no. 1, pp. 51–57, 2008.

[32] W. Chen and S. Huang, "Human reliability analysis for visual inspection in aviation maintenance by a bayesian network approach," *Transportation Research Record*, vol. 2449, no. 1, pp. 105–113, 2014.

[33] M. P. Enright and D. M. Frangopol, "Condition prediction of deteriorating concrete bridges using Bayesian updating," *Journal of Structural Engineering*, vol. 125, no. 10, pp. 1118–1125, 1999.

[34] G. Papaefthymiou and B. Klockl, "MCMC for wind power simulation," *IEEE Transactions on Energy Conversion*, vol. 23, no. 1, pp. 234–240, 2008.

[35] L. Gundry, S.-X. Guo, G. Kennedy, J. Keith, M. Robinson, D. Gavaghan, A. M. Bond, and J. Zhang, "Recent advances and future perspectives for automated parameterisation, bayesian inference and machine learning in voltammetry," *Chemical Communications*, vol. 57, no. 15, pp. 1855–1870, 2021.

[36] J. Wang and X. Liu, "Evaluation and Bayesian dynamic prediction of deterioration of structural performance," *Structure and Infrastructure Engineering*, vol. 6, no. 6, pp. 663–674, 2010.

[37] T.-B. Tran, E. Bastidas-Arteaga, and F. Schoefs, "Improved Bayesian network configurations for probabilistic identification of degradation mechanisms: application to chloride ingress," *Structure and Infrastructure Engineering*, vol. 12, no. 9, pp. 1162–1176, 2016.

[38] A. Kosgodagan-Dalla Torre, T. G. Yeung, O. Morales-Nápoles, B. Castanier, J. Maljaars, and W. Courage, "A two-dimension dynamic Bayesian network for large-scale degradation modeling with an application to a bridges network," *Computer-Aided Civil and Infrastructure Engineering*, vol. 32, no. 8, pp. 641–656, 2017.

[39] M. I. Jordan, *Learning in graphical models*. MIT press, 1999.

[40] C. M. Bishop, *Pattern recognition and machine learning*. Springer, 2006.

[41] R. E. Kalman, "Contributions to the theory of optimal control," *Bol. Soc. Mat. Mexicana*, vol. 5, no. 2, pp. 102–119, 1960.

[42] I. T. Jolliffe, *Principal components in regression analysis*. Springer, 1986, pp. 129–155.

[43] H. E. Rauch, C. Striebel, and F. Tung, "Maximum likelihood estimates of linear dynamic systems," *AIAA journal*, vol. 3, no. 8, pp. 1445–1450 0001–1452, 1965.

[44] D. Simon and D. L. Simon, "Constrained Kalman filtering via density function truncation for turbofan engine health estimation," *International Journal of Systems Science*, vol. 41, no. 2, pp. 159–171 2010.

[45] J. Bennetts, G. Webb, S. Denton, P. Vardanega, and N. Loudon, "Quantifying uncertainty in visual inspection data," *Maintenance, Safety, Risk, Management and Life-Cycle Performance of Bridges*, pp. 2252–2259, 2018.

[46] N. Burlutskiy, M. Petridis, A. Fish, A. Chernov, and N. Ali, *An investigation on online versus batch learning in predicting user behaviour*. Springer, 2016.

[47] R. I. Jennrich and S. M. Robinson, "A newton-raphson algorithm for maximum likelihood factor analysis," *Psychometrika*, vol. 34, no. 1, pp. 111–123, 1969.

[48] J.-A. Goulet, L. H. Nguyen, and S. Amiri, "Tractable approximate Gaussian inference for Bayesian neural networks," *Journal of Machine Learning Research*, vol. 22, no. 251, pp. 1533–7928, 2021.

[49] Y. Bar-Shalom, X. R. Li, and T. Kirubarajan, *Estimation with applications to tracking and navigation: theory algorithms and software.* John Wiley and Sons, 2004.

[50] J.-A. Goulet, *Probabilistic machine learning for civil engineers.* MIT Press, 2020.

APPENDIX A TRANSFORMATION FUNCTION FOR SSM DETERIORATION MODEL

The proposed transformation function $o^{-1}(.)$ is defined for the domain $x \in (0, \infty]$; to have a function defined for $x \in [-\infty, \infty]$,

$$\tilde{x} = o^{-1}(x) = \begin{cases} \frac{1}{\Gamma(\alpha)} \int_0^{x^{\frac{1}{\alpha}}} t^{\alpha-1} e^{-t} dt, & x > \frac{u+l}{2}, \\ x, & x = \frac{u+l}{2}, \\ -\frac{1}{\Gamma(\alpha)} \int_0^{x^{\frac{1}{\alpha}}} t^{\alpha-1} e^{-t} dt, & x < \frac{u+l}{2}, \end{cases} \tag{A.1}$$

where $\tilde{x}$ represents the state in the constrained space $\tilde{x} \in [l, u]$.
The transformation function $o(.)$ mapping the state $\tilde{x} \in [l, u]$ to $x \in [-\infty, \infty]$ is defined by,

$$x = o(\tilde{x}) = \begin{cases} \left[\frac{1}{\Gamma(\alpha)} \int_0^{\tilde{x}} t^{\alpha-1} e^{-t} dt \right]^{\alpha}, & \frac{u+l}{2} < \tilde{x} \leq u, \\ \tilde{x}, & \tilde{x} = \frac{u+l}{2}, \\ -\left[\frac{1}{\Gamma(\alpha)} \int_0^{\tilde{x}} t^{\alpha-1} e^{-t} dt \right]^{\alpha}, & l \leq \tilde{x} < \frac{u+l}{2}, \end{cases} \tag{A.2}$$

where the parameter α is given by: $\alpha = 2^{-n}$, with n is a positive integer $n \in \mathbb{Z}^+$. The role of the parameter n is to control the curvature at the transformation function ends.

APPENDIX B GRADIENT-BASED PARAMETER ESTIMATION FRAMEWORK FOR SSM-KR DETERIORATION MODEL

Algorithm 1 Gradient-based parameter estimation framework for SSM-KR

Require: $\boldsymbol{\theta}_0^s$: Initial SSM parameters
Require: $\boldsymbol{\theta}_0^k, \dot{\boldsymbol{x}}_{\boldsymbol{z}}$: Initial KR parameters and state respectively
$L_1 \leftarrow -10^{12}$ (Initial *log-likelihood*), $\epsilon \leftarrow 0.999$ (Convergence tolerance)
$\rho_1 \leftarrow 10, \rho_2 \leftarrow 10$ (Stall limits)
$\zeta_1 \leftarrow 1$, $\zeta_2 \leftarrow 1$ (Initial stall),
$\nu_1 \leftarrow 300, \nu_2 \leftarrow 1$ (Iteration limit per parameter)
$\boldsymbol{\theta}_1^s \leftarrow \text{NewtonRaphson}(\mathcal{L}(\boldsymbol{\theta}^s), \boldsymbol{\theta}_0^s, \nu_1)$
$\sigma_V(I_{1:\mathtt{I}}) = \sigma_V,\ \sigma_V \in \boldsymbol{\theta}_1^s$
$\mu_V(I_{1:\mathtt{I}}) = 0$
$L_2 \leftarrow \mathcal{L}(\boldsymbol{\theta}_1^s)$
$j \leftarrow 1$
while $(L_{j+1}/L_j) \leq \epsilon$ or $\zeta_1 \geq \rho_1$ **do**
    while $(L_{j+1}/L_j) \leq \epsilon$ or $\zeta_2 \geq \rho_2$ **do**
        $L_j \leftarrow L_{j+1}$
        for $i := 1$ to $\mathtt{I}$ **do**
            if $j = 1$ **then**
                $\mu_V(I_i), \sigma_V(I_i) \leftarrow \text{NewtonRaphson}(\mathcal{L}(\mu_V(I_i), \sigma_V(I_i)), \boldsymbol{\theta}_j^s, \nu_2)$
            else $\mu_V(I_i), \sigma_V(I_i) \leftarrow \text{NewtonRaphson}(\mathcal{L}(\mu_V(I_i), \sigma_V(I_i), \dot{\boldsymbol{x}}_{\boldsymbol{z}}), \boldsymbol{\theta}_j^s, \nu_2)$
        $L_{j+1} \leftarrow \mathcal{L}(\mu_V(I_i), \sigma_V(I_{1:\mathtt{I}}))$
        if $(L_{j+1}/L_j) \leq 0.05$ **then**
            $\zeta_2 = \zeta_2 + 1$
    if $j = 1$ **then**
        $\boldsymbol{\theta}_{j+1}^s \leftarrow \text{NewtonRaphson}(\mathcal{L}(\boldsymbol{\theta}_j^s), \boldsymbol{\theta}_j, \nu_1)$
    else $\boldsymbol{\theta}_{j+1}^s \leftarrow \text{NewtonRaphson}(\mathcal{L}(\boldsymbol{\theta}_j^s, \dot{\boldsymbol{x}}_{\boldsymbol{z}}), \boldsymbol{\theta}_j, \nu_1)$
    $[\boldsymbol{\theta}_{j+1}^k, \dot{\boldsymbol{x}}_{\boldsymbol{z}}] \leftarrow \text{NewtonRaphson}(\mathcal{L}(\boldsymbol{\theta}_j^k, \text{RecursiveEstimation}(\dot{\boldsymbol{x}}_{\boldsymbol{z}})), \boldsymbol{\theta}_j, \nu_1)$
    $L_j \leftarrow \mathcal{L}(\boldsymbol{\theta}_{j+1})$
    $\zeta_1 = \zeta_1 + 1$, $j = j + 1$
return $\boldsymbol{\theta}_{j+1}$ and $\dot{\boldsymbol{x}}_{\boldsymbol{z}}$ (Resulting parameters)

APPENDIX C INCORPORATION OF THE ANALYTICAL METHOD WITHIN THE ESTIMATION FRAMEWORK FOR THE SSM-KR MODEL

Algorithm 2 Incorporation of the Analytical Method within the estimation framework for the SSM-KR model

Require: $\boldsymbol{\theta}_0^s$: Initial SSM parameters
Require: $\boldsymbol{\theta}_0^k, \dot{\boldsymbol{x}}_{\boldsymbol{z}}$: Initial KR parameters and state respectively
Require: $\boldsymbol{x}_0, \ddot{\boldsymbol{x}}_0$: Initial state for condition and acceleration

$L_1 \leftarrow -10^{12}$ (Initial *log-likelihood*), $\epsilon \leftarrow 0.999$ (Convergence tolerance)
$\boldsymbol{\theta}_1^s \leftarrow \text{NewtonRaphson}(\mathcal{L}(\boldsymbol{\theta}^s), \boldsymbol{\theta}_0^s, \nu_1)$
$\mu_{V_s}(I_{1:\mathtt{I}}) = \sigma_V,\ \sigma_V \in \boldsymbol{\theta}_1^s,\ \sigma_{V_b}(I_{1:\mathtt{I}}) = 12$
$\mu_{V_b}(I_{1:\mathtt{I}}) = 0,\ \sigma_{V_b}(I_{1:\mathtt{I}}) = 1$
$L_2 \leftarrow \mathcal{L}(\boldsymbol{\theta}_1^s)$
$j \leftarrow 1$
while $(L_{j+1}/L_j) \leq \epsilon$ **do**
    while $(L_{j+1}/L_j) \leq \epsilon$ **do**
        $L_j \leftarrow L_{j+1}$
        for $p := 1$ to $\mathtt{E}$ **do**
            for $t := 1$ to $\mathtt{T}$ **do**
                if $j = 1$ **then**
                $\mu_V(I_i), \sigma_V(I_i), \boldsymbol{x}_{t+1,p} \leftarrow \text{AnalyticalFramework}(y_{t,p}, \boldsymbol{x}_{t,p}, \boldsymbol{\theta}_j^s)$
                else
                $\mu_V(I_i), \sigma_V(I_i), \boldsymbol{x}_{t+1,p} \leftarrow \text{AnalyticalFramework}(y_{t,p}, \boldsymbol{x}_{t,p}, \boldsymbol{\theta}_j^s, \boldsymbol{\theta}_j^k, \dot{\boldsymbol{x}}_{\boldsymbol{z}})$
        $L_{j+1} \leftarrow \mathcal{L}(\mu_V(I_i), \sigma_V(I_{1:\mathtt{I}}))$
    if $j = 1$ **then**
        $\boldsymbol{\theta}_{j+1}^s \leftarrow \text{NewtonRaphson}(\mathcal{L}(\boldsymbol{\theta}_j^s), \boldsymbol{\theta}_j, \nu_1)$
    else $\boldsymbol{\theta}_{j+1}^s \leftarrow \text{NewtonRaphson}(\mathcal{L}(\boldsymbol{\theta}_j^s, \dot{\boldsymbol{x}}_{\boldsymbol{z}}), \boldsymbol{\theta}_j, \nu_1)$
    $[\boldsymbol{\theta}_{j+1}^k, \dot{\boldsymbol{x}}_{\boldsymbol{z}}] \leftarrow \text{NewtonRaphson}(\mathcal{L}(\boldsymbol{\theta}_j^k, \text{RecursiveEstimation}(\dot{\boldsymbol{x}}_{\boldsymbol{z}})), \boldsymbol{\theta}_j, \nu_1)$
    $L_j \leftarrow \mathcal{L}(\boldsymbol{\theta}_{j+1})$
    $j \leftarrow j + 1$
return $\boldsymbol{\theta}_{j+1}$ and $\dot{\boldsymbol{x}}_{\boldsymbol{z}}$ (Resulting parameters)

APPENDIX D SSM-KR ESTIMATED MODEL PARAMETERS

In this appendix, the estimated model parameters are presented for each framework based on inspection data from the synthetic or real database.

Table D.1 Estimation of SSM-KR model parameters for synthetic inspection data using the gradient-based framework.

σ_W	σ_0	σ_V	$\ddot{\sigma}_0$	p_1	p_2	n	σ_{w0}	ℓ^{RBF}
5.3×10^{-3}	1.5834	3.001	0.0499	0.0252	0.14997	4	0.1322	0.1439

Table D.2 Estimation of SSM-KR model parameters for synthetic inspection data using the analytical framework.

σ_W	σ_0	σ_V	$\ddot{\sigma}_0$	p_1	p_2	n	σ_{w0}	ℓ^{RBF}
5.43×10^{-3}	1.477	3.001	0.0499	0.0252	0.14996	4	0.1776	0.1811

Table D.3 Estimation of SSM-KR model parameters for real data using the gradient-based framework.

σ_w	σ_0^x	σ_V	$\sigma_0^{\ddot{x}}$	p_1	p_2	n
4.543×10^{-3}	$1,0212$	$2,385$	0.0499	0.02447	0.1499	4
σ_{w_0}	$\ell^{\texttt{AAK}}$	$\ell^{\texttt{M12}}$	$\ell^{\texttt{M12}}$	$\ell^{\texttt{M52}}$		
0.1028	0.050	22.40	0.9918	7.0218		

Table D.4 Estimation of SSM-KR model parameters for real data using the analytical framework.

σ_w	σ_0^x	σ_V	$\sigma_0^{\ddot{x}}$	p_1	p_2	n
5.384×10^{-3}	1	2.385	0.0499	0.0254	0.1499	4
σ_{w_0}	$\ell^{\texttt{AAK}}$	$\ell^{\texttt{M12}}$	$\ell^{\texttt{M12}}$	$\ell^{\texttt{M52}}$		
0.1390	0.05	23.289	1.0402	6.3541		